

Methane emissions from the Nord Stream subsea pipeline leaks

<https://doi.org/10.1038/s41586-024-08396-8>

Received: 4 December 2023

Accepted: 30 October 2024

Published online: 15 January 2025

Open access

 Check for updates

Stephen J. Harris^{1✉}, Stefan Schwietzke^{1,2}, James L. France^{2,3}, Nataly Velandia Salinas², Tania Meixus Fernandez¹, Cynthia Randles¹, Luis Guanter^{2,4}, Itziar Irakulis-Loitxate^{1,4}, Andreea Calcan^{1✉}, Ilse Abern^{5,6}, Katarina Abrahamsson⁷, Paul Balcombe⁸, Antoine Berchet⁹, Louise C. Biddle¹⁰, Henry C. Bittig¹¹, Christian Böttcher¹², Timo Bouvard¹³, Göran Broström⁷, Valentin Bruch¹⁴, Massimo Cassiani¹⁵, Martyn P. Chipperfield^{16,17}, Philippe Ciais⁹, Ellen Damm¹⁸, Enrico Dammers¹⁹, Hugo Denier van der Gon¹⁹, Matthieu Dogniaux⁵, Emily Dowd^{16,17}, François Dupouy¹³, Sabine Eckhardt¹⁵, Nikolaos Evangelios¹⁵, Wuhu Feng^{17,20}, Mengwei Jia²¹, Fei Jiang²¹, Andrea K. Kaiser-Weiss¹⁴, Ines Kamoun⁹, Brian J. Kerridge^{22,23}, Astrid Lampert²⁴, José Lana²⁵, Fei Li²¹, Joannes D. Maasakkers⁵, Jean-Philippe W. Maclean²⁶, Buhalgem Mamtimin¹⁴, Julia Marshall²⁷, Gédéon Mauger¹³, Anouar Mekkas¹³, Christian Mielke¹², Martin Mohrmann¹⁰, David P. Moore^{28,29}, Riccardo Nanni¹⁹, Falk Pätzold²⁴, Isabelle Pison⁹, Ignacio Pisso¹⁵, Stephen M. Platt¹⁵, Raphaël Prêa¹³, Bastien Y. Queste⁷, Michel Ramonet⁹, Gregor Rehder¹¹, John J. Remedios^{28,29}, Friedemann Reum²⁷, Anke Roiger²⁷, Norbert Schmidbauer¹⁵, Richard Siddans^{22,23}, Anusha Sunkisala¹⁴, Rona L. Thompson¹⁵, Daniel J. Varon³⁰, Lucy J. Ventress^{22,23}, Chris Wilson^{16,17} & Yuzhong Zhang³¹

The amount of methane released to the atmosphere from the Nord Stream subsea pipeline leaks remains uncertain, as reflected in a wide range of estimates^{1–18}. A lack of information regarding the temporal variation in atmospheric emissions has made it challenging to reconcile pipeline volumetric (bottom-up) estimates^{1–8} with measurement-based (top-down) estimates^{8–18}. Here we simulate pipeline rupture emission rates and integrate these with methane dissolution and sea-surface outgassing estimates^{9,10} to model the evolution of atmospheric emissions from the leaks. We verify our modelled atmospheric emissions by comparing them with top-down point-in-time emission-rate estimates and cumulative emission estimates derived from airborne¹¹, satellite^{8,12–14} and tall tower data. We obtain consistency between our modelled atmospheric emissions and top-down estimates and find that 465 ± 20 thousand metric tons of methane were emitted to the atmosphere. Although, to our knowledge, this represents the largest recorded amount of methane released from a single transient event, it is equivalent to 0.1% of anthropogenic methane emissions for 2022. The impact of the leaks on the global atmospheric methane budget brings into focus the numerous other anthropogenic methane sources that require mitigation globally. Our analysis demonstrates that diverse, complementary measurement approaches are needed to quantify methane emissions in support of the Global Methane Pledge¹⁹.

Subsea natural gas leaks from pipeline ruptures and well blowouts can emit large quantities of methane (CH₄) to the ocean and atmosphere. Prominent examples are the 22/4b well blowout^{20,21}, the Deepwater Horizon oil disaster^{22,23} and the Elgin rig blowout²⁴. The Nord Stream 1 and 2 twin pipeline systems (NS1 and NS2) are a network of offshore pipelines underlying the Baltic Sea that connect the Russian natural gas supply with Europe^{25–27}. On 26 September 2022, damage to both NS1 and NS2 occurred in a series of underwater explosions, resulting in the leakage of natural gas (Fig. 1). The first explosion occurred at 00:03 UTC southeast of the Danish Island of Bornholm in the Bornholm Basin, rupturing pipeline A of the twin NS2 pipeline system (NS2A) at approximately 70 m depth^{28–30}. This explosion destroyed approximately 10 m

of the pipeline³¹. At 17:03 UTC, multiple explosions to the northeast of Bornholm ruptured both NS1 pipelines (NS1A and NS1B) at depths of approximately 75 m (ref. 30) and caused a smaller partial rupture in the NS2A pipeline to the north of the previous NS2A leak^{31,32}. These explosions destroyed 200–300 m of the NS1A and NS1B pipelines³¹. The NS2B pipeline remained undamaged³³.

Although not operational at the time, both NS1 and NS2 pipeline systems were filled with pressurized natural gas^{1–5}. The natural gas released from the ruptured pipelines was predominantly CH₄ along with small amounts of ethane, nitrogen and other hydrocarbons³⁴. The emitted gas was seen bubbling through the sea surface above the four rupture sites, creating bulging mounds of foamy seawater of up

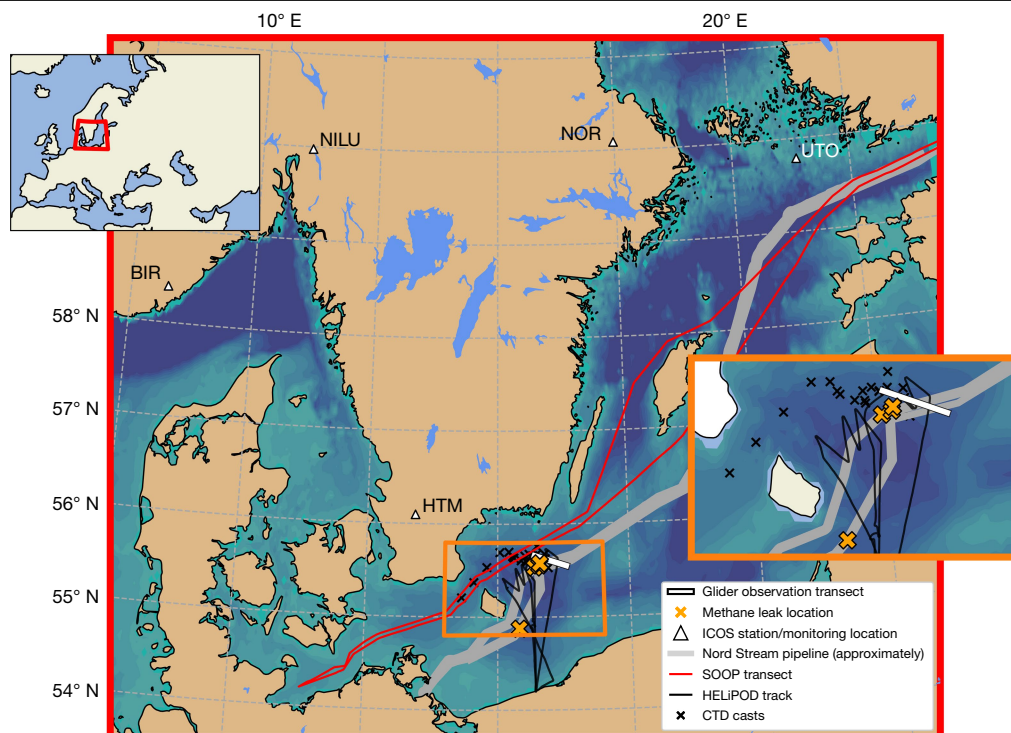


Fig. 1 | Location of the Nord Stream gas leak sites in the Baltic Sea. The first rupture occurred to the southeast of Bornholm on NS2A (54° 52.6' N, 15° 24.6' E)²⁸. The remaining three ruptures occurred to the northeast of Bornholm on NS1A (55° 33.4' N, 15° 47.3' E)³², NS1B (55° 32.1' N, 15° 41.9' E)³² and NS2A (55° 32.45' N, 15° 46.47' E)³². The locations of marine (SOOP, ocean glider and CTD, see text) and airborne (HELIPOD, see text) observations are depicted. The inset map on

the right offers a detailed view of the sampling locations for the CTD casts, ocean glider and HELIPOD observations near the leak sites. The tall towers located at the ICOS BIR, HTM, NOR and UTO observatory stations and an atmospheric monitoring location located at the Norwegian Institute for Air Research (NILU) in Kjeller are shown. The ICOS ZEP observatory station is located to the north of the map area in Svalbard, Norway.

to several hundred metres in diameter, which lasted for approximately 1 week. Given the magnitude, persistence and visibility of the emitted gas, there was an immediate desire to estimate the amount of CH₄ emitted to the atmosphere to understand the potential environmental and climatic impact^{1–5}.

A wide range of bottom-up and top-down approaches were used to estimate the various components of CH₄ emissions from the event (Supplementary Table 1). Bottom-up pipeline emissions estimates, quantifying the amount of CH₄ contained in (or released from) the pipelines before (or after) rupturing, were derived from volumetric calculations and simulations based on pipeline physical parameters and information from pipeline operators^{1–8}. Top-down estimates, quantifying the amount of CH₄ released from the pipelines to the Baltic Sea and atmosphere, were derived from marine and ship-based measurements^{9,10}; airborne in situ measurements¹¹; satellite measurements^{8,12–14}; and atmospheric CH₄ measurements captured by tall tower observatory stations within the European Integrated Carbon Observation System (ICOS)^{8,15–18}. Top-down approaches had varying spatiotemporal coverage of the leaks and used a diverse set of measurement platforms. The top-down approaches used to inform our analysis are shown in Fig. 2.

Reported bottom-up estimates across the three ruptured pipelines range from 230 to 509 thousand metric tons (kt) of CH₄ (refs. 1–8). An initial report in February 2023 documenting top-down estimates concluded that 75–230 kt of CH₄ was emitted to the atmosphere³⁵. However, cautious interpretation of these initial bottom-up and top-down estimates is required because of the methodological limitations and assumptions inherent to each approach, as well as the need to contextualize the estimates in both space and time. Supplementary Table 1 presents all available bottom-up and top-down estimates, including those reported in this paper, and outlines the limitations and contributions of each approach to quantifying atmospheric CH₄ emissions from the leaks.

Here we integrate bottom-up pipeline rupture emission-rate simulations with marine CH₄ dissolution estimates⁹ to model the time series of atmospheric emissions from the leaks. We verify our simulated atmospheric emission rates over time by comparing them with point-in-time atmospheric emission-rate estimates derived from airborne measurements¹¹ and point-source imaging satellites^{8,12,13}, as well as cumulative emissions estimates, acquired from atmospheric inversion methods using satellite and tall tower observations that incorporate revised a priori (prior) atmospheric emission rates. Agreement between our simulated atmospheric emissions and top-down atmospheric estimates across multiple spatiotemporal domains demonstrates that our synthesis provides a more reliable estimate of atmospheric CH₄ emissions from the leaks than previous studies.

Emissions from the ruptured pipelines

Using the volume of natural gas in each pipeline (Extended Data Table 1) and its composition (Extended Data Table 2), we estimate that 496 ± 14 kt of CH₄ was contained in the three pipelines before rupturing (Methods and Extended Data Table 3). Subsequently, we use PBREAK³⁶ and the Code for Analysis of Thermal Hydraulics during Accident and for Reactor safety Evaluation (CATHARE)³⁷ to simulate post-rupture pipeline CH₄ emission rates from NS1A, NS1B and NS2A (Methods and Supplementary Method 1). In both simulations, pipeline CH₄ emission rates from NS1A and NS1B are each about 1×10^5 t h⁻¹ in the seconds after rupturing (Extended Data Fig. 1). These decrease to about 1×10^4 t h⁻¹ after 2 h and about 1×10^3 t h⁻¹ over the following 2 days. Pipeline emission rates from NS2A are about 7×10^4 t h⁻¹ in the initial seconds, decreasing to about 1×10^4 t h⁻¹ after 30 min and about 1×10^3 t h⁻¹ after 30 h. The potential impact of the partial northern rupture in NS2A on emission rates from the southern NS2A leak site is probably minor (Supplementary Discussion 1). PBREAK modelling indicates that leaking

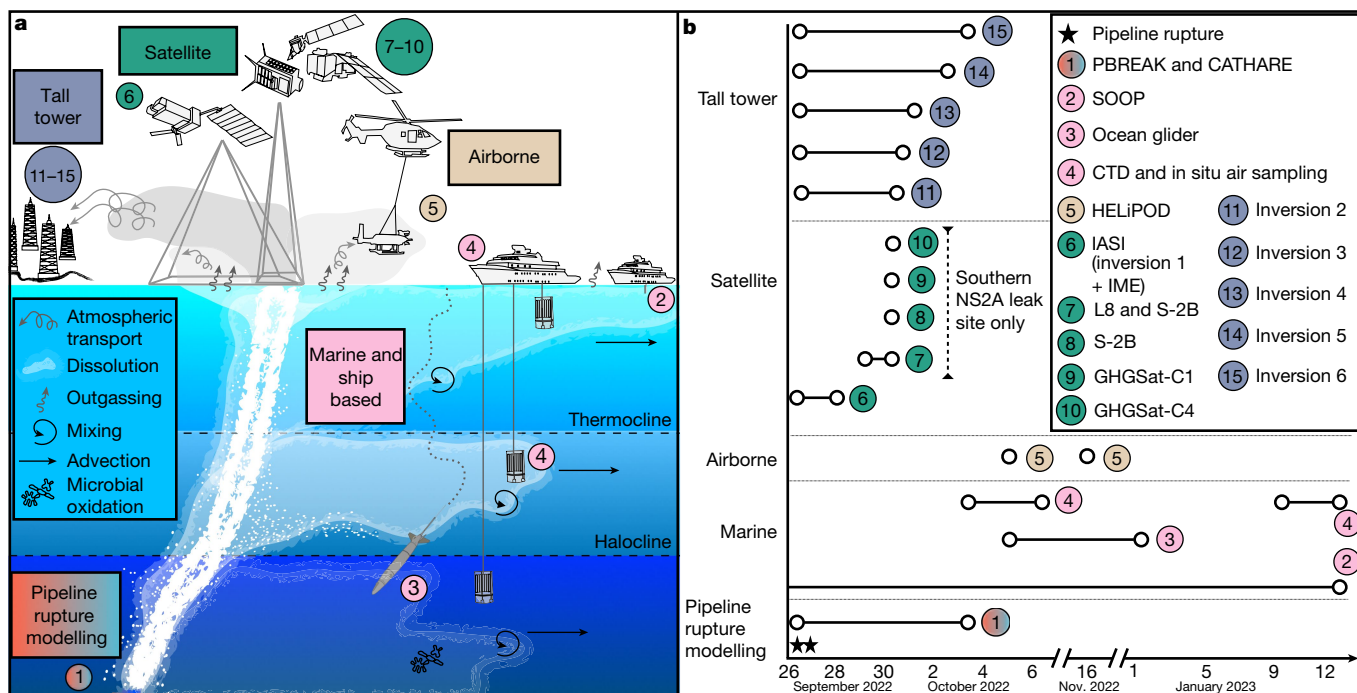


Fig. 2 | Overview of measurement approaches applied in our analysis and the period(s) over which the measurements were taken. a, Bottom-up and top-down measurement approaches applied in our analysis of the Nord Stream pipeline leaks. The numbers 1–15 correspond to each measurement approach. **b**, The period(s) over which the measurements were taken. See text and Supplementary Table 1 for details on each approach. Although shown, the

results of a second airborne campaign on 16 and 17 November 2022 using HELiPOD, and a second marine campaign deploying CTD casts between 9 and 12 January 2023 have not been published and are not otherwise available. MetOp-B and Sentinel-2B satellite icons adapted with permission from the European Space Agency (ESA) and ESA/ATG Medialab. GHGSat Satellite icon adapted from GHGSat.

stopped on 1 October for NS2A and on 2 October for NS1A and NS1B. These timelines are consistent with reports that the pressure in NS2A stabilized on 1 October³⁸, and sea foam patch observations indicating that bubbling at the NS1A leak site had ceased by 06:00 UTC on 3 October (A. Sundberg, personal communication). CATHARE modelling suggests leaking extended one day longer compared with PBREAK. Nonetheless, time series of landfall pipeline pressures simulated using CATHARE are broadly consistent with reports from pipeline operators (Extended Data Fig. 2). CH₄ hydrate formation was unlikely to impact our simulated pipeline emission rates (Supplementary Discussion 2).

Our PBREAK simulations estimate that a total of 457 ± 14 kt of CH₄ was released from the pipelines following the ruptures. CATHARE modelling indicates a larger total of 472 ± 14 kt. From both simulations, we estimate 23 ± 1 kt remained within the three pipelines once pressure stabilized at the seafloor (Extended Data Table 3) and, of this, <1 kt was subsequently displaced by seawater (Extended Data Fig. 2). The differences between pre-rupture pipeline inventories and post-rupture estimates of CH₄ contained in the pipelines are used to derive discrepancies in the total mass of CH₄ released from the pipelines in our simulations (Extended Data Table 3). Owing to its lower mass discrepancy, we consider the CATHARE estimate (472 ± 14 kt) to be a more accurate estimation of CH₄ released from the 3 ruptured pipelines (Supplementary Discussion 3).

Marine and ship-based estimates

At each rupture site, the leaked gas was transported to the sea surface via rapidly ascending plumes of bubbles³⁹. During this period, the Bornholm Basin showed strong vertical temperature and salinity gradients creating a distinct three-layer system separated by a thermocline (about 30–40 m depth) and halocline (about 50 m depth)^{9,10}. During its ascent through the water column, a fraction of the CH₄ was dissolved, advected and mixed in each of the three layers (Fig. 2a). A fraction of

the dissolved CH₄ was outgassed to the atmosphere via air–sea gas exchange from the mixed surface layer. The presence of a thermocline and halocline during this time inhibited direct mixing between seawater layers and resulted in the build-up of dissolved CH₄ at mid-depths⁹. By January 2023, the seawater column shifted to a two-layer structure in the absence of a thermocline, vertically deepening the mixed surface layer and facilitating further outgassing of dissolved CH₄ (refs. 9,10).

The shallow depth of the ruptures (70–80 m) allowed the plumes to rise quickly through the water column, causing only a small fraction of the total CH₄ released from the pipelines to dissolve. Microbial CH₄ oxidation was probably most prominent below the halocline, where ventilation to the atmosphere is minimal, and the highest abundance of indigenous methanotrophic communities is found in the Bornholm Basin⁴⁰. This contrasts with the Deepwater Horizon blowout, where a substantial component of the CH₄ had dissolved in deep seawater (>1,000 m depth), which allowed large quantities of CH₄ to undergo oxidation in the water column²³.

Dissolved CH₄ concentrations were continuously measured near the northernmost leaks between 5 October 2022 and 2 January 2023 using an autonomous SeaExplorer glider equipped with a Franatech METS CH₄ sensor⁹ (Figs. 1 and 2, and Supplementary Method 2). Concurrently, sea-surface CH₄ partial pressures were measured using an underway analytical system onboard the ship of opportunity (SOOP) *Finnmaid* (DE-SOOP-Finnmaid), which passed the leak sites twice every 3 days. The glider and SOOP observations were used to establish the vertical and horizontal subsea CH₄ plume structures and set initial conditions for an oceanic chemical fate and transport model driven by the PBREAK and CATHARE pipeline emission rates derived from the present study. The modelling suggests between 9 kt and 15 kt of the CH₄ released from the ruptured pipelines was dissolved in the Baltic Sea, of which 8–13 kt was outgassed to the atmosphere at rates of up to 74 t h^{-1} (Fig. 3).

The seawater column near the northernmost leaks was sampled for dissolved CH₄ concentrations and stable carbon isotopic signatures

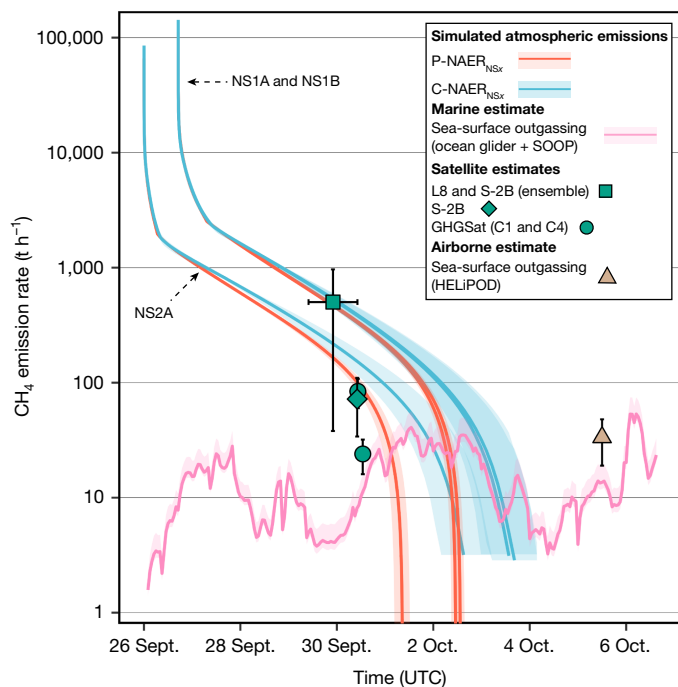


Fig. 3 | Net atmospheric CH₄ emission rates. The net atmospheric CH₄ emission rates were derived using PBREAK (P-NAER_{NSx}; orange) and CATHARE (C-NAER_{NSx}; blue) for the NS1A, NS1B and NS2A pipelines compared with top-down emission rates. The shaded regions represent the upper and lower uncertainty bounds for P-NAER_{NSx}, C-NAER_{NSx} and sea-surface outgassing⁹. Satellite estimates^{8,12,13} are only comparable to the NS2A emission rates. The error bars on the y-axis for satellite estimates represent 1σ standard deviation. The x-axis error bars for the L8 and S-2B ensemble estimate represent the time span between the two satellite detections. The symbol and error bars for the airborne estimate represent the central (average) estimate and range reported in ref. 11, respectively. It is noted that sea-surface outgassing rates modelled by ref. 9 extend beyond 6 October 2022, which are not shown here.

between 3 and 5 October 2022 using conductivity, temperature and depth (CTD) casts deployed from the RV *Skagerak*¹⁰ (Figs. 1 and 2, and Supplementary Method 3). Subsea plume simulations, corroborated by fossil CH₄ isotopic signatures, suggest that 9% of dissolved CH₄ from the ruptured pipelines was transported by currents to 16 of 20 sampling sites. Using the average and maximum dissolved CH₄ concentration measured across sampling sites, the amount of dissolved CH₄ was extrapolated to be 10 kt and 55 kt, respectively¹⁰. In our analysis, we consider the 10-kt estimate to be more credible because maximum dissolved CH₄ concentrations did not persist over all sampling locations. Atmospheric CH₄ concentrations were also measured onboard RV *Skagerak* near several CTD sampling sites using a Picarro G2132-i laser spectrometer¹⁰. Estimated sea-surface CH₄ outgassing rates ranged from $0.5 \times 10^{-3} \text{ t h}^{-1} \text{ km}^{-2}$ and $5 \times 10^{-3} \text{ t h}^{-1} \text{ km}^{-2}$. Although providing further evidence of outgassing, these rates have not been spatially modelled beyond the extent of CTD sampling sites to other regions shown to have undergone outgassing^{9,11}, thus limiting their ability to inform gross outgassing rates over the Baltic Sea.

Bottom-up bubble-plume simulations suggest that about 11 kt of the CH₄ released from the ruptured pipelines was dissolved in the Baltic Sea, of which about 3 kt was oxidized and about 8 kt outgassed to the atmosphere³⁹. However, this modelling assumes that 215 kt of CH₄ was released from the pipelines (Supplementary Table 1). Our modelling indicates over twice this amount was released from the pipelines. Therefore, we refrain from using these estimates in our analysis, except for providing an estimate of microbial CH₄ oxidation based on the percentage relative to total pipeline emissions (about 1%)³⁹.

Simulated atmospheric emissions

Satellite and tall tower observations^{8,14–18} showed that once the CH₄ had escaped the water column, the plumes were transported across various parts of Scandinavia and the North Sea between 26 September and 1 October. Our simulated pipeline emission rates cannot be directly compared with top-down quantifications of these plumes because they do not account for CH₄ dissolution in the water column during the plumes' ascent. Consequently, we use modelled CH₄ dissolution rates⁹ to calculate the CH₄ emission rate expected to reach the atmosphere directly from each pipeline (NS_x), called herein the net atmospheric emission rate (P-NAER_{NSx} for PBREAK and C-NAER_{NSx} for CATHARE; Methods and Fig. 3). We also calculated the combined sum of net atmospheric emissions from all three pipelines (P-NAE_{All} and C-NAE_{All}; Methods and Fig. 4), to allow for direct comparison with satellite and tall tower inversion approaches, which do not distinguish between the total amount of atmospheric CH₄ emissions from the individual pipelines.

Comparison with atmospheric measurements

Airborne estimate

Atmospheric CH₄ concentration enhancements and meteorological parameters near all leak sites were measured on 5 October 2022 using the helicopter borne sonde HELiPOD⁴¹ equipped with a Picarro G2401-m laser spectrometer¹¹ (Figs. 1 and 2, and Supplementary Method 4). An emission rate of $19\text{--}48 \text{ t h}^{-1}$ was derived using an inverse model of atmospheric transport. By 5 October, the pipeline leaks had ceased, meaning the atmospheric CH₄ enhancements measured by HELiPOD were derived from the outgassing of dissolved CH₄ rather than from direct emission via bubbling. Thus, no direct comparison with P-NAER_{NSx} and C-NAER_{NSx} can be made. Nonetheless, considering random uncertainties, the lower bound ($19 \pm 5 \text{ t h}^{-1}$) is consistent with the glider and SOOP outgassing estimate on 5 October⁹ ($11\text{--}18 \text{ t h}^{-1}$; Fig. 3).

Satellite point-source estimates

The Planet, Landsat 8 (L8), GF5-02-AHSI, Sentinel-2 and Sentinel-1 satellite platforms acquired imagery of the pipeline leak sites between 26 September and 1 October⁸. However, emission-rate quantification was achieved for only the southern NS2A leak on 29 and 30 September using L8 and Sentinel-2B (S-2B) nadir observations^{8,12} and sun-glint measurements with the GHGSat constellation¹³. Over sea, the reflected signal detected by Earth-surface imaging satellites is ordinarily too low at nadir to detect any useful CH₄ signal. However, the bright patch of sea foam caused by the NS2A leak created enough reflectance to detect CH₄ using L8 and S-2B. The NS1A, NS1B and northern NS2A leaks could not be sampled by high-resolution satellites owing to cloud coverage during the entire emission event.

An emission rate of $72 \pm 38 \text{ t h}^{-1}$ was derived by applying the integrated mass enhancement (IME) method⁴² to S-2B nadir observations over the southern NS2A leak on 30 September at 10:07 UTC⁸ (Fig. 2 and Supplementary Method 5). The upper range of this estimate is consistent with P-NAER_{NSx} ($86\text{--}115 \text{ t h}^{-1}$; Fig. 3 and Extended Data Table 4). An emission rate of $502 \pm 464 \text{ t h}^{-1}$ was also derived by applying multi-band single-pass⁴³ and specifically calibrated IME methods⁴² to L8 and S-2B satellite nadir observations over the southern NS2A leak on 29 September (09:56 UTC) and 30 September (10:07 UTC)¹² (Fig. 2 and Supplementary Method 6). This estimate addresses methodological limitations detailed in ref. 8 by using a calibration procedure that accounts more rigorously for spectral interferences from sea-surface bubbling, and provides a comprehensive uncertainty estimate. The lower range of this estimate is consistent with P-NAER_{NS2A} ($85\text{--}258 \text{ t h}^{-1}$; Fig. 3 and Extended Data Table 4).

Three plume detections of the southern NS2A leak were obtained from available cloud-free acquisitions from the GHGSat constellation at 08:51, 10:26 and 12:54 UTC on 30 September (GHGSat-C2, -C1 and

-C4, respectively) using a sun-glint configuration¹³ (Fig. 2 and Supplementary Method 7). An emission rate for the C2 observation was not achieved because the signal was too low (high scattering angle and low surface reflectivity). The C1 observation had the highest signal of the three observations, and comprised a steady streamlined plume that spanned the length of the observation¹³. The emission rate for C1 ($84 \pm 24 \text{ t h}^{-1}$) is within 1σ uncertainty of P-NAER_{NS2A} ($84\text{--}113 \text{ t h}^{-1}$; Fig. 3 and Extended Data Table 4). In contrast, the plume detected in C4 had a lower signal strength compared with C1 and comprised a more dispersed plume, possibly owing to increased atmospheric turbulence, as emission rates slowed near the later stages of the leak. These factors may contribute to discrepancies between the C4 emission rate ($24 \pm 8 \text{ t h}^{-1}$) and P-NAER_{NS2A} ($72\text{--}101 \text{ t h}^{-1}$; Fig. 3 and Extended Data Table 4). The next clear-sky GHGSat observation was on 3 October, which indicated that the leak had subsided.

Satellite estimates using IASI

The Infrared Atmospheric Sounding Interferometer (IASI) onboard Eumetsat's MetOp-B satellite detected elevated CH₄ over the Baltic Sea around 07:30 UTC on 26 September¹⁴. CH₄ plumes were either not or only partially visible from space as they moved over land owing to cloud cover over Scandinavia later on 26 and 27 September. However, on 28 September, IASI observed large enhancements ($>200 \text{ ppb}$) of column averaged CH₄ (XCH₄) off the west coast of Norway. Using their own emission priors, ref. 14 combined the XCH₄ enhancements with an atmospheric transport model in an inversion framework to obtain an estimate of 219–427 kt. Here we re-evaluate these results using P-NAER_{NSX} and C-NAER_{NSX} as priors (inversion 1; Methods). Our revised posterior atmospheric emission of 281–346 kt has reduced uncertainty compared with the initial estimate and is consistent with equivalent P-NAE_{All} and C-NAE_{All} until 28 September (311–326 kt and 301–336 kt; Fig. 4 and Extended Data Table 4).

The IME method was also applied to IASI XCH₄ enhancements to derive an estimate of $30 \pm 1 \text{ kt}$ on 26 September¹⁷. Although this is broadly consistent with P-NAE_{All} and C-NAE_{All}, similarly derived estimates on 27 and 28 September ($16 \pm 1 \text{ kt}$, and $161 \pm 4 \text{ kt}$ and $77 \pm 2 \text{ kt}$) are lower than P-NAE_{All} and C-NAE_{All} (Extended Data Table 4). We note the IME method as applied by ref. 14 cannot account for IASI's vertical sensitivity, which is highest in the upper troposphere, and that these enhancements may comprise only partial plume observations owing to cloud cover (Supplementary Table 1). Both methodological limitations can lead to an underestimate of atmospheric emissions, preventing us from using these quantifications to verify our simulated atmospheric emissions.

Tall tower inversion estimates

Regionally enhanced atmospheric CH₄ concentrations were detected across multiple tall towers within the ICOS observation network, including the Norunda (NOR), Hyltemossa (HTM), Birkenes (BIR), Utö-Baltic Sea (UTO) and Zeppelin (ZEP) observatory stations, and a station located in Kjeller, Norway (Figs. 1 and 2). Atmospheric monitoring stations in Finland and Estonia also detected CH₄ enhancements⁶. Unfortunately, enhancements from the Nord Stream plumes were detected for only short periods (Extended Data Fig. 4) because wind directions frequently changed during the event. Moreover, their narrow structure meant small changes in the advecting field moved the plumes away from the stations. Relating simulated plumes to the ICOS observations has proved challenging^{6,8,15–18}, particularly because of meteorological uncertainty, which can lead to large spatiotemporal errors in each plume's location (for example, Extended Data Fig. 5), as well as uncertainty in the plume injection height above each leak site⁶. It is also noteworthy that the automated processing routines for the near-real-time ICOS tall tower data had filtered out very high CH₄ concentrations, which are now included in Level 2 release ICOS CH₄ time series⁴⁴ (Extended Data Fig. 4). Nonetheless, attempts were

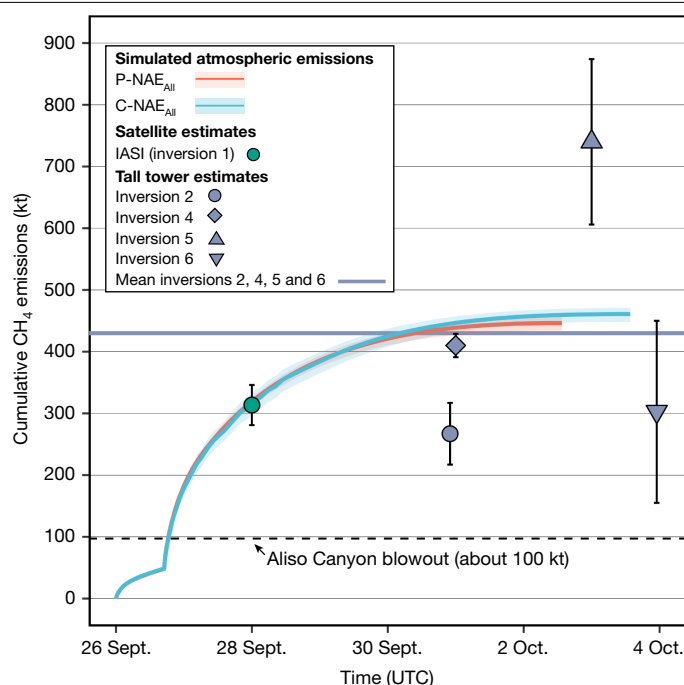


Fig. 4 | Comparison of net atmospheric emissions derived using PBREAK and CATHARE with satellite and tall tower estimates used in our analysis.

Total CH₄ emissions from the Aliso Canyon blowout⁴⁵ are shown for comparison. The symbols and error bars for inversions 1, 2 and 4–6 represent central (average) estimates and ranges, respectively. It is noted that initial tall tower inverse estimates are not plotted here, nor inversion 3, which derives only a minimum estimate of atmospheric CH₄ emissions (see text and Supplementary Table 1).

made to provide initial atmospheric emissions estimates using various inversion frameworks to near-real-time ICOS observations applying constant^{8,15,16} and exponential^{17,18} priors. Central estimates from these initial approaches range from 56 kt to 226 kt, with a mean ($\pm 1\sigma$) of $165 \pm 64 \text{ kt}$ (refs. 8,15–18; Supplementary Table 1).

Here we report five tall tower inversion estimates using quality-controlled ICOS CH₄ time series⁴⁴ that apply P-NAER_{NSX} and/or C-NAER_{NSX} as the prior (inversions 2–6; Methods). Inversions 2, 4 and 6 are reanalyses of previous inversions^{8,16–18}. Our inversions use a range of atmospheric transport models and are driven by different meteorological data at varying model resolutions. Apart from inversion 3, which derives a lower bound of atmospheric emissions up to 1 October ($\geq 230 \text{ kt}$; Methods), central estimates from inversions 2, 4, 5 and 6 range from 267 kt to 716 kt CH₄, with a mean ($\pm 1\sigma$) of $430 \pm 216 \text{ kt}$. Although our mean estimate has large uncertainty, it is consistent with P-NAE_{All} and C-NAE_{All} (434–456 kt and 448–471 kt; Fig. 4 and Extended Data Table 4). The mean difference of approximately 265 kt between our estimates and those in the literature illustrates the reliance of atmospheric inversion models on emission priors, especially when observations are sparse. We acknowledge that our mean estimate is caveated because it assumes equal performance across our inversions, which is unlikely given the methodologies varied (Supplementary Table 1). For example, the sparsity of observations leads to an overestimation in inversion 5 ($740 \pm 134 \text{ kt}$; Supplementary Discussion 4), which skews our mean estimate upwards. Notably, inversion 6 (155–450 kt), which uses a Bayesian data assimilation approach to quantify uncertainty in both the plume location based on an ensemble of meteorological forecasts and injection heights based on gas velocity rates from CATHARE simulations, is compatible with P-NAE_{All} and C-NAE_{All}.

Total atmospheric CH₄ emissions

Using our modelled pipeline emissions in conjunction with marine estimates of dissolution, outgassing and microbial oxidation, we

Table 1 | Atmospheric CH₄ emissions budget from the Nord Stream pipeline leaks

Emission component	CH ₄ (kt)
Pre-rupture pipeline inventory ^a	496 ± 14
Pipeline NS1A	191 ± 5
Pipeline NS1B	191 ± 5
Pipeline NS2A	114 ± 3
Pipeline CH ₄ emissions (CH ₄ pipeline emissions) ^b	472 ± 14
Pipeline NS1A ^b	183 ± 5
Pipeline NS1B ^b	183 ± 5
Pipeline NS2A ^b	106 ± 3
CH ₄ remaining in pipelines ^c	23 ± 1
CH ₄ displaced by seawater in pipelines (CH ₄ displaced pipeline) ^d	<1
CH ₄ dissolved in Baltic Sea (CH ₄ dissolved) ^e	9–15
Sea-surface outgassing (CH ₄ outgassed) ^f	8–13
Microbial CH ₄ oxidation (CH ₄ oxidized) ^g	6
Total atmospheric CH ₄ emissions (CH ₄ atmospheric total) ^h	446–485
Total atmospheric CH ₄ emissions ⁱ	465 ± 20

Differences of 1 kt of CH₄ in the totals can occur owing to rounding errors. ^aCorresponds to the amount of CH₄ initially contained within the three pipelines before rupturing. See Methods and Extended Data Table 3. ^bWe use the CATHARE estimate for the cumulative emissions estimate owing to its lower total cumulative mass discrepancy (Extended Data Table 3 and Supplementary Discussion 3). ^cSee Extended Data Table 3. ^dSee Extended Data Fig. 3. In the emissions budget calculation, this is assumed to equal 1 kt of CH₄. ^eMinimum and maximum ranges derived from ref. 9 (9–15 kt) and ref. 10 (10 kt) CH₄ dissolution estimates. See text for details. ^fMinimum and maximum ranges of outgassing derived from ref. 9. ^gBased on percentage biodegradation (1.3% of total emissions) estimated by ref. 39. ^hMinimum range computed as: min(CH₄ atmospheric total) = min(CH₄ pipeline emissions) + CH₄ displaced pipeline – max(CH₄ dissolved) + min(CH₄ outgassed) – CH₄ oxidized. Maximum range computed as: max(CH₄ atmospheric total) = max(CH₄ pipeline emissions) + CH₄ displaced pipeline – min(CH₄ dissolved) + max(CH₄ outgassed) – CH₄ oxidized. ⁱCentral estimate of CH₄ atmospheric total. Rounded to the nearest 5 kt.

conservatively estimate that 465 ± 20 kt of CH₄ was emitted to the atmosphere from the Nord Stream pipeline leaks (Table 1). Our simulated time series of atmospheric emissions broadly align with airborne, satellite and tall tower estimates over various points in time and space (Figs. 3 and 4, and Extended Data Table 4), indicating that this estimate is consistent with the available ensemble of atmospheric quantifications. Our analysis confirms that, to our knowledge, the leaks were the largest recorded emission of CH₄ to the atmosphere from a single transient event. Our estimate is over 4 times greater than atmospheric emissions from the previous largest natural gas leak at the Aliso Canyon storage facility (approximately 100 kt of CH₄)⁴⁵. Remarkably, emissions from the 4-month-long Aliso Canyon leak were surpassed within just 1 day (Fig. 4). Despite their magnitude on short-term timescales, atmospheric emissions from the leaks are equivalent to about 1.2% of emissions from the natural gas sector, and only 0.3% of CH₄ emissions from agriculture, for 2022⁴⁶. Moreover, they amount to only 0.1% of anthropogenic CH₄ emissions for 2022⁴⁶. Equally, the small impact of the leaks on the anthropogenic CH₄ budget highlights the large number of other CH₄ sources that require mitigation globally.

Top-down analysis of the event proved challenging because the leaks were short-lived and occurred near-simultaneously across four separate offshore locations. Time was needed to deploy instruments^{9–11} and task satellites to the leak sites, and there were several occasions where cloud coverage prevented satellite quantification^{8,12–14}. This meant that some parts of the event were missed by individual approaches (Fig. 2). Importantly, the plumes were not transported consistently over tall tower monitoring stations, leading to considerable uncertainty across inversion estimates. These methodological constraints limit our ability to rely solely on top-down approaches to estimate the atmospheric emissions from the event (Supplementary Table 1). Nonetheless, the

collective ensemble of top-down quantifications offers an invaluable way of ensuring that our modelled atmospheric emissions are reliable. More generally, our analysis highlights the benefits of applying diverse measurement approaches to verify bottom-up estimates in support of CH₄ reduction commitments such as the Global Methane Pledge¹⁹. Developing and maintaining a varied measurement toolkit that allows for rapid detection and quantification of future ultra-emitter events—whether transient or persistent—remains an essential requirement to support meeting these ambitious targets.

Online content

Any methods, additional references, Nature Portfolio reporting summaries, source data, extended data, supplementary information, acknowledgements, peer review information; details of author contributions and competing interests; and statements of data and code availability are available at <https://doi.org/10.1038/s41586-024-08396-8>.

1. Leaks in Nord Stream 1 and 2 will cause serious climate damage. *German Environment Agency* <https://www.umweltbundesamt.de/en/press/pressinformation/leaks-in-nord-stream-1-2-will-cause-serious-climate> (2022).
2. Sanderson, K. What do Nord Stream methane leaks mean for climate change? *Nature News* <https://doi.org/10.1038/d41586-022-03111-x> (2022).
3. Plejdrup, M. S. *Emission Calculations for Leaks on the Nord Stream 1 and 2 Pipelines* [in Danish] (Aarhus University, DCE – National Center for Environment and Energy, 2023).
4. Gas-Leaks bei Nord Stream 1 & 2. *Leibniz Institute for Baltic Sea Research Warnemünde* <https://www.io-warnemuende.de/short-news-archiv-details/items/gas-leaks-bei-nord-stream-1-2.html> (2022).
5. The possible climate effect of the gas leaks from the Nord Stream 1 and Nord Stream 2 pipelines. *Danish Energy Agency* <https://ens.dk/en/press/possible-climate-effect-gas-leaks-nord-stream-1-and-nord-stream-2-pipelines> (2022).
6. Kouznetsov, R. et al. A bottom-up emission estimate for the 2022 Nord Stream gas leak: derivation, simulations, and evaluation. *Atmos. Chem. Phys.* **24**, 4675–4691 (2024).
7. Poursanidis, K., Sharanik, J. & Hadjistassou, C. World's largest natural gas leak from nord stream pipeline estimated at 478,000 tonnes. *iScience*. **27**, 108772 (2024).
8. Jia, M. et al. The Nord Stream pipeline gas leaks released approximately 220,000 tonnes of methane into the atmosphere. *Environ. Sci. Ecotech.* **12**, 100210 (2022).
9. Mohrmann, M., Biddle, L. C., Rehder, G., Bittig, H. & Queste, B. Y. Nord Stream methane leaks spread across 14% of Baltic waters. *Nat. Commun.* <https://doi.org/10.1038/s41467-024-53779-0> (2025).
10. Abrahamsson, K. et al. Methane plume detection after the 2022 Nord Stream pipeline explosion in the Baltic Sea. *Sci. Rep.* **14**, 12848 (2024).
11. Reum, F. et al. Airborne observations reveal the fate of the methane from the Nord Stream pipelines. *Nat. Commun.* <https://doi.org/10.1038/s41467-024-53780-7> (2025).
12. Dogniaux, M., Maasakkers, J. D., Varon, D. J. & Aben, I. Report on Landsat 8 and Sentinel-2B observations of the Nord Stream 2 pipeline methane leak. *Atmos. Meas. Tech.* **17**, 2777–2787 (2024).
13. MacLean, J.-P. W. et al. Offshore methane detection and quantification from space using sun glint measurements with the GHGSat constellation. *Atmos. Meas. Tech.* **17**, 863–874 (2024).
14. Wilson, C. et al. Quantifying large methane emissions from the Nord Stream pipeline gas leak of September 2022 using IASI satellite observations and inverse modelling. *Atmos. Chem. Phys.* **24**, 10639–10653 (2024).
15. CAMS simulates methane emissions from Nord Stream pipelines leaks. *Copernicus Atmosphere Monitoring Service* <https://atmosphere.copernicus.eu/cams-simulates-methane-emissions-nord-stream-pipelines-leaks> (2022).
16. Orjollé, S. Nord Stream leaked less methane than feared: atmospheric monitor. *Phys.org* <https://phys.org/news/2022-10-nord-stream-leaked-methane-atmospheric.html> (2022).
17. Ramonet, M., Berchet, A., Pison, I. & Ciais, P. Suivi du panache de méthane émis par les fuites des gazoducs Nord Stream en mer Baltique. *La Météorologie* **119**, 6–8 (2022).
18. Solbakken, C. F. Improved estimates of Nord Stream leaks. *NILU* <https://www.nilu.com/2022/10/improved-estimates-of-nord-stream-leaks/> (2022).
19. *Global Methane Pledge* (UNEP CCAC, 2021); <https://www.ccacoalition.org/resources/global-methane-pledge>.
20. von Deimling, J. S., Linke, P., Schmidt, M. & Rehder, G. Ongoing methane discharge at well site 22/4b (North Sea) and discovery of a spiral vortex bubble plume motion. *Mar. Pet. Geol.* **68**, 718–730 (2015).
21. Rehder, G., Keir, R. S., Suess, E. & Pohlmann, T. The multiple sources and patterns of methane in North Sea waters. *Aquat. Geochem.* **4**, 403–427 (1998).
22. Yvon-Lewis, S. A., Hu, L. & Kessler, J. Methane flux to the atmosphere from the Deepwater Horizon oil disaster. *Geophys. Res. Lett.* **38**, L01602 (2011).
23. Kessler, J. D. et al. A persistent oxygen anomaly reveals the fate of spilled methane in the deep Gulf of Mexico. *Science* **331**, 312–315 (2011).
24. Lee, J. D. et al. Flow rate and source reservoir identification from airborne chemical sampling of the uncontrolled Elgin platform gas release. *Atmos. Meas. Tech.* **11**, 1725–1739 (2018).
25. Operations. *Nord Stream AG* <https://www.nord-stream.com/operations/> (2023).
26. *Esposo Report Ch. 4: Description of the Project* (Nord Stream AG, 2009); https://www.nord-stream.com/press-info/library/?per_page=100&q=&type=3&category=&country=.
27. *Background Information* (Nord Stream AG, 2016); <https://www.nord-stream.com/download/document/10/?language=en>.

28. *Navigational Warning: The Baltic Sea NW-230-22* (Danish Maritime Authority, 2022); https://nautiskinformation.sofartsstyrelsen.dk/details.pdf?messa_geld=72b2c3b1-OdOd-4a14-9ee0-be96c0a699fb&language=en.
29. GEUS has registered tremors in the Baltic Sea. *Geological Survey of Denmark and Greenland* <https://www.geus.dk/om-geus/nyheder/nyhedsarkiv/2022/sep/seismologi> (2022).
30. *European Marine Observation and Data Network (EMODnet): Bathymetry Data* (European Commission, 2023); <https://emodnet.ec.europa.eu/en>.
31. Botnariuc, L. et al. Investigating the Nord Stream Attack. *SPIEGEL International* <https://www.spiegel.de/international/europe/investigating-the-attack-on-nord-stream-all-the-clues-point-towa-rd-kyiv-a-124838c7-992a-4d0e-9894-942d4a665778> (2023).
32. *Navigational Warning: The Baltic Sea NW-235-22* (Danish Maritime Authority, 2022); https://nautiskinformation.sofartsstyrelsen.dk/details.pdf?mes_sageld=8166360e-4f40-4b43-b2a1-4aa81f9f1552&language=en.
33. Ringstrom, A. Gazprom lowers pressure in undamaged part of Nord Stream 2 pipe, Denmark says. *Reuters* <https://www.reuters.com/business/energy/gazprom-lowers-pressure-undamaged-part-nord-stream-2-pipe-denmark-says-2022-10-05/> (2022).
34. *Erdgas - Orientierungswerte 2021* (Open Gas Europe, 2022); https://gitfront.io/r/StephenHarrisUNEPIMEO/E_mq51iMoNq3M/Available-Data-for-Harris-et-al-Methane-emissions-from-the-Nord-Stream-subsea-pipeline-leaks/.
35. *Estimate of Total Methane Emissions from the Nord Stream Gas Leak Incident Draft Working Paper* (United Nations Environment Programme & International Methane Emissions Observatory, 2023); <https://wedocs.unep.org/20.500.11822/41838>.
36. Acton, M., Baldwin, P., Baldwin, T. & Jager, E. The development of the PIPESAFE risk assessment package for gas transmission pipelines. In *Proc. 1998 2nd International Pipeline Conference 1-7* (ASME, 1998).
37. Préa, R. et al. CATHARE-3 V2.1: the new industrial version of the CATHARE code. In *ATH'20—Advances in Thermal Hydraulics 2020* <https://cea.hal.science/cea-04087378> (American Nuclear Society, 2020).
38. Danes: Nord Stream 2 pipeline seems to have stopped leaking. *Associated Press* <https://apnews.com/article/russia-ukraine-putin-united-states-germany-business-afebd99d298ac72192acfeabfe384609> (2022).
39. Dissanayake, A. L., Gros, J., Drews, H. J., Nielsen, J. W. & Drews, A. Fate of methane from the Nord Stream pipeline Leaks. *Environ. Technol. Lett.* **10**, 903–908 (2023).
40. Schmale, O. et al. Distribution of methane in the water column of the Baltic Sea. *Geophys. Res. Lett.* **37**, L12604 (2010).
41. Pätzold, F. et al. HELIPOD—revolution and evolution of a helicopter borne measurement system for multidisciplinary research in demanding environments. *Elem. Sci. Anth.* **11**, 00031 (2023).
42. Varon, D. J. et al. Quantifying methane point sources from fine-scale satellite observations of atmospheric methane plumes. *Atmos. Meas. Tech.* **11**, 5673–5686 (2018).
43. Varon, D. J. et al. High-frequency monitoring of anomalous CH₄ point sources with multispectral Sentinel-2 satellite observations. *Atmos. Meas. Tech.* **14**, 2771–2785 (2021).
44. ICOS RI et al. ICOS atmosphere release 2023-1 of level 2 greenhouse gas mole fractions of CO₂, CH₄, N₂O, CO, meteorology and ¹⁴CO₂, and flask samples analysed for CO₂, CH₄, N₂O, CO, H₂ and SF₆. *ICOS* <https://doi.org/10.18160/VXCS-95EV> (2023).
45. Conley, S. et al. Methane emissions from the 2015 Aliso Canyon blowout in Los Angeles, CA. *Science* **351**, 1317–1320 (2016).
46. *Global Methane Tracker 2023* (IEA, 2023); <https://www.iea.org/reports/global-methane-tracker-2023>.

Publisher's note Springer Nature remains neutral with regard to jurisdictional claims in published maps and institutional affiliations.



Open Access This article is licensed under a Creative Commons Attribution-NonCommercial-NoDerivatives 4.0 International License, which permits any non-commercial use, sharing, distribution and reproduction in any medium or format, as long as you give appropriate credit to the original author(s) and the source, provide a link to the Creative Commons licence, and indicate if you modified the licensed material. You do not have permission under this licence to share adapted material derived from this article or parts of it. The images or other third party material in this article are included in the article's Creative Commons licence, unless indicated otherwise in a credit line to the material. If material is not included in the article's Creative Commons licence and your intended use is not permitted by statutory regulation or exceeds the permitted use, you will need to obtain permission directly from the copyright holder. To view a copy of this licence, visit <http://creativecommons.org/licenses/by-nc-nd/4.0/>.

© United Nations Environment Programme and the Authors 2025

¹United Nations Environment Programme's International Methane Emissions Observatory (UNEP's IMEO), Paris, France. ²Environmental Defense Fund Europe, Brussels, Belgium. ³Department of Earth Sciences, Royal Holloway, University of London, Egham, UK. ⁴Research Institute of Water and Environmental Engineering (IIAMA), Universitat Politècnica de València, Valencia, Spain. ⁵SRON Netherlands Institute for Space Research, Leiden, The Netherlands. ⁶Department of Earth Sciences, Vrije Universiteit Amsterdam, Amsterdam, The Netherlands. ⁷Department of Marine Sciences, University of Gothenburg, Gothenburg, Sweden. ⁸School of Engineering and Material Science, Queen Mary University of London, London, UK. ⁹Laboratoire des Sciences du Climat et de l'Environnement, LSCE/IPSL, CEA-CNRS-UVSQ, Université Paris-Saclay, Gif-sur-Yvette, France. ¹⁰Voice of the Ocean Foundation, Västra Frölunda, Sweden. ¹¹Department of Marine Chemistry, Leibniz Institute for Baltic Sea Research Warnemünde (IOW), Rostock, Germany. ¹²German Environment Agency, Dessau-Rosslau, Germany. ¹³Université Paris-Saclay, CEA, Service de Thermo-hydraulique et de Mécanique des Fluides, Gif-sur-Yvette, France. ¹⁴Deutscher Wetterdienst, Offenbach, Germany. ¹⁵NILU, Kjeller, Norway. ¹⁶National Centre for Earth Observation, University of Leeds, Leeds, UK. ¹⁷School of Earth and Environment, University of Leeds, Leeds, UK. ¹⁸Alfred Wegener Institute for Polar and Marine Research, Bremerhaven, Germany. ¹⁹Department of Air Quality and Emissions Research, TNO, Utrecht, The Netherlands. ²⁰National Centre for Atmospheric Science (NCAS), University of Leeds, Leeds, UK. ²¹Jiangsu Provincial Key Laboratory of Geographic Information Science and Technology, International Institute for Earth System Science, Nanjing University, Nanjing, China. ²²National Centre for Earth Observation, STFC Rutherford Appleton Laboratory (RAL), Chilton, UK. ²³Remote Sensing Group, STFC Rutherford Appleton Laboratory, Chilton, UK. ²⁴Technische Universität Braunschweig, Institute of Flight Guidance, Braunschweig, Germany. ²⁵Enagás Transportes SAU, Madrid, Spain. ²⁶GHGSat Inc., Montreal, Quebec, Canada. ²⁷Deutsches Zentrum für Luft- und Raumfahrt e.V. (DLR), Institut für Physik der Atmosphäre, Oberpfaffenhofen, Germany. ²⁸National Centre for Earth Observation, University of Leicester, Leicester, UK. ²⁹School of Physics and Astronomy, University of Leicester, Leicester, UK. ³⁰School of Engineering and Applied Sciences, Harvard University, Cambridge, MA, USA. ³¹Key Laboratory of Coastal Environment and Resources of Zhejiang Province, School of Engineering, Westlake University, Hangzhou, China. ³²e-mail: stephen.harris@un.org; andreea.calcan@un.org

Methods

Pre-rupture pipeline inventories

We estimate the mass of CH₄ contained in each pipeline before rupturing using equation (1):

$$M_{NSx} = L_{NSx} \times \rho_{NSx} \times 0.25 \times D_{NSx}^2 \times \pi \times C_{NSx} / 1,000 \quad (1)$$

where M_{NSx} is the mass of CH₄ contained within pipeline NSx (kt of CH₄), L_{NSx} is the total pipeline length in kilometres (km), ρ_{NSx} is the density of the natural gas mixture at the pressure and temperature within the pipeline (kg m⁻³), D_{NSx} is the pipeline diameter (m), and C_{NSx} is the percentage mass composition of CH₄ in the natural gas (Extended Data Tables 1 and 2). In equation (1), we use ρ_{NSx} values from the gas mixture eventually used in the PBREAK simulations because our CATHARE simulations do not consider components in the mixture that make up less than 0.1% (Extended Data Table 2).

Pipeline emission simulation tools

We use PBREAK³⁶ (version 2.28.3) and CATHARE (version CATHARE-3³⁷) to simulate pipeline rupture emission from NS1A, NS1B and NS2A. PBREAK is a mathematical model used to simulate the outflow of gas following the sudden puncture or rupture of a high-pressure transmission pipeline^{36,47–49}. The model is embedded in the PIPESAFE Quantitative Risk Assessment software. CATHARE is a tool developed by the French Alternative Energies and Atomic Energy Commission used for thermal hydraulic simulations of multiphase flows (<https://cathare.cea.fr>)^{37,50–53}. Both model pipeline depressurization as the one-dimensional flow of natural gas in a pipeline and solve a system of three conservation equations for mass, momentum and energy. The models use an equation of state to compute fluid properties (Supplementary Discussion 3). Further descriptions of each model, including their suitability for modelling subsea pipeline ruptures, are provided in Supplementary Method 1.

PBREAK

Within the PBREAK workflow, each pipeline is divided in N segments, and the nonlinear equations for continuity and mass balance, momentum and energy solved at each time step using an implicit finite-difference scheme³⁶. These equations are solved every 1 s for the first 2 min, then every 30 s until the calculation finishes. The computation terminates when the internal pressure in all the lengths of each pipeline is equal to the external pressure. The model results are the variation with time of the outflow at the point of rupture coming from each branch of pipeline, and the cumulative flow from the beginning of the release.

CATHARE

We discretize each of the three pipelines into one-dimensional elements meshed with a series of cylinders. We define the cross-section (A), friction perimeter (χ_f) and roughness of the pipelines. In the case of monophasic calculations, CATHARE solves a system with three main variables (pressure P , enthalpy H and velocity V) and three conservation equations (equations (2)–(4): conservation of mass, momentum and energy):

$$A \times \frac{\partial \rho}{\partial t} + \frac{\partial (A \times \rho \times V)}{\partial z} = 0 \quad (2)$$

$$A \times \rho \times \left(\frac{\partial V}{\partial t} + V \times \frac{\partial V}{\partial z} \right) + A \times \frac{\partial P}{\partial z} = - \chi_f \times C_f \times \rho \times \frac{V|V|}{2} + A \times \rho \times g_z \quad (3)$$

$$A \times \frac{\partial}{\partial t} \left[\rho \times \left(H + \frac{V^2}{2} \right) \right] + \frac{\partial}{\partial z} \left[A \times \rho \times V \times \left(H + \frac{V^2}{2} \right) \right] - A \times \frac{\partial P}{\partial t} = \chi_c \times q_w + A \times \rho \times V \times g_z \quad (4)$$

We add thermal structure to each of the cylinders by specifying their heating perimeter (χ_c). The heat conduction through the wall structures is resolved by a multilayer radial discretization and we define the heat exchange with an external fluid. The pipelines are assumed to be horizontal (gravity projection g_z equal to 0 in equations (3) and (4)).

The one-dimensional elements use a first-order finite-volume scheme with a staggered mesh and the donor-cell principle. The time discretization is fully implicit. The mass and energy equations in CATHARE use a conservative form and are discretized to ensure mass and energy conservation. The wall conduction is implicitly coupled with the hydraulic calculations. The nonlinear system of equations is solved in several steps using an iterative Newton–Raphson method. The numerical resolution allows the model to consider sonic flow as a boundary condition during the pipeline rupturing.

The fluid equation of state is computed by coupling CATHARE with the REFPROP library from the National Institute of Standards and Technology⁵⁴, which uses the GERG-2008 equation of state⁵⁵ to compute properties (such as density ρ) for natural gas mixtures. We use two closure laws to model the interaction between the internal fluid and the pipe wall. Given the high gas velocity and the large pipe diameter, the flow is deemed fully turbulent throughout the transient (Reynold's number exceeding 3,000). Therefore, the wall friction coefficient (C_f) is evaluated using the Colebrook factor⁵⁶. The convective wall heat transfer (q_w) is modelled using the Colburn correlation⁵⁷.

To simulate the rupture, we use a numerical methodology previously applied to flow pipe breaks in a pressurized water reactor. As per previous applications, a very fine mesh of 10⁻⁵ m is used at the break side. From this point, the mesh size is gradually increased with a 1.05 adjacent cell size ratio up to 500 m, and then is kept constant until the other end. In the initial state, the velocity is zero all along the pipe and the pressure and temperature are initialized at their initial values. At the rupture location point, the pressure drops from the initial pressure to the outlet pressure (hydrostatic pressure at the seafloor) value in 10⁻³ s. To minimize the computation time, the time step at the beginning of the rupture is set to 10⁻⁵ s and progressively increased to 10⁻⁴ s. This procedure is applied to each side of the three pipelines to evaluate the evolution of the total gas flow rate as a function of time.

Sensitivity analysis

We assess uncertainty in our simulations by reperforming the PBREAK and CATHARE simulations using the upper and lower uncertainty bounds for the initial gas temperature, depth of rupture, post-rupture pipeline section lengths and natural gas composition (Extended Data Table 1). As the variables are independent, we sum the resulting deviations from reference emission rates in quadrature to derive the uncertainty at each time step of the simulation. We additionally assess the model uncertainty in CATHARE simulations by varying pipeline roughness, heat transfer coefficients, mesh number and break size (Supplementary Method 1). The CATHARE model uncertainties are summed in quadrature in addition to the uncertainties introduced by the model variables. We do not assess the model uncertainty in PBREAK as this functionality is not accessible to users of the software.

NAER and NAE

We calculate the rate of CH₄ emission expected to directly reach the atmosphere (NAER) from each pipeline (NSx) over time, according to equation (5):

$$X\text{-NAER}_{NSx} = r_{NSx,t} - d_{NSx,t} \quad (5)$$

where X- is the simulation (P- for PBREAK and C- for CATHARE), t is the simulation time step, n is the total number of simulation time steps, r is

the pipeline CH₄ emission rate (t h⁻¹), and d is the CH₄ dissolution rate⁹ for the equivalent simulation time step (t h⁻¹). We compute equation (5) over the lower and upper uncertainty bounds of the pipeline emission rates to derive lower and upper bounds of P-NAER_{NSX} and C-NAER_{NSX}. In our paper, we use P-NAER_{NSX} for comparison with top-down atmospheric emission-rate estimates because the pipeline emission rates derived from PBREAK modelling align better with timelines reported by the pipeline operators³⁸ and leak site observations (A. Sundberg, personal communication). The cumulative sum of net atmospheric emissions for each pipeline and pipeline emission-rate simulation (P-NAE_{NSX} and C-NAE_{NSX}, in kt of CH₄) is calculated using equation (6):

$$X\text{-NAE}_{\text{NSX}} = \sum_{t=1}^n (r_{\text{NSX},t} - d_{\text{NSX},t}) \quad (6)$$

We sum the atmospheric CH₄ emissions from all three pipeline leaks to derive P-NAE_{All} and C-NAE_{All}.

Inversion 1

Inversion 1 is derived from the reanalysis of a previous inversion¹⁴ (Supplementary Table 1). Briefly, IASI XCH₄ data retrievals^{58,59} are combined with simulated mixing ratios produced by the TOMCAT offline chemical transport model⁶⁰ in an inversion framework to optimally quantify the flux rate from the leaks. A global model simulation is carried out covering the period of 26–30 September 2022. The model's horizontal resolution is approximately 1° × 1°, with 60 vertical levels between the surface and 0.1 hPa. The model dynamical time step is 5 min. The model is initialized with CH₄ mixing ratios from ref. 61, which are optimized in the inversion. The fluxes of CH₄ from sources other than the Nord Stream leaks are also based on that study, as are the atmospheric loss rates.

Here, both P-NAER_{NSX} and C-NAER_{NSX} and their uncertainties are used as priors in the inversions. Leak flux rates in each emission window (the first 5 min of each leak, the remainder of the first hour and then subsequent 3-h periods) are treated as constant within that window. To drive model transport, meteorological data from the European Centre for Medium-range Weather Forecasts (ECMWF) operational analyses are applied at the same horizontal resolution as the model. In total, we perform eight inversions using the P-NAER_{NSX} and C-NAER_{NSX} priors, with each one optimized against all individual IASI retrievals, or alternatively optimized against the mean XCH₄ value in the region of the observed plume, with prior error covariances also tested. Our estimate represents the range across these eight inversions.

Inversion 2

Inversion 2 is derived from the reanalysis of a previous inversion¹⁸ (Supplementary Table 1), using CH₄ concentrations from three ICOS stations (BIR, NOR and ZEP)^{62–64} and the Norwegian Institute for Air Research (NILU) between 26 and 30 September 2022. The Lagrangian Particle Dispersion Model FLEXPART⁶⁵ is used to model atmospheric transport and is driven by meteorological data obtained from the ECMWF Integrated Forecasting System. A synthesis inversion approach assuming Gaussian errors is employed for the inverse modelling⁶⁶. CH₄ enhancements are derived by subtracting the average of time-series CH₄ concentrations immediately before and after the plume passed at each station. We assemble the CH₄ enhancements in an observation vector y and corresponding hourly emission rates into a state vector x and solve for the optimal estimation of x by minimizing the cost function $J(x)$ in equation (7):

$$J(x) = (x - x_b)^T B^{-1} (x - x_b) + (Hx - y)^T R^{-1} (Hx - y) \quad (7)$$

where x_b is the prior estimate, T denotes the operation of matrix transposition, B is the prior error covariance matrix, H is the Jacobian matrix operator constructed using FLEXPART transport simulations, y is the

concentration enhancement with respect to the background, and R is the observational covariance matrix. The optimal solution to equation (7) (\hat{x}) is given by:

$$\hat{x} = x_b + BH^T (HBH^T + R)^{-1} (y - Hx_b) \quad (8)$$

The previous estimate¹⁸ used wind data at 1° resolution, and x_b were derived by modelling flow rates from the depressurization based on initial reports of the pipeline volume, temperature, and pressure in the NS2A pipeline². Here we use wind data at 0.2° resolution and both P-NAER_{NSX} and C-NAER_{NSX} for x_b . Both forwards and backwards simulations are used. Error correlations of 10% for R are used for the inversions based on forward simulations, with no off-diagonal entries being non-zero. Simulations are produced for the transport operator H in forward mode at different resolutions. To account for the uncertainty in the prior, we perform six inversions using the upper, central and lower bounds of P-NAER_{NSX} and C-NAER_{NSX}. In addition, we estimate transport uncertainty using a variant of the statistical technique of resampling. We perform an initial inversion using all available time series for each station and then subsample the stations to obtain inversions using the same inversion parameters. We report the range across estimates derived using this approach.

Inversion 3

Inversion 3 is derived using CH₄ concentrations from four ICOS stations (BIR, NOR, HTM and UTO)^{62,67–69} and the NILU between 26 September and 1 October 2022. We use the numerical weather prediction (NWP) model Icosahedral Non-hydrostatic Aerosols and Reactive Trace gases (ICON-ART)^{70,71} to model atmospheric transport. The model is run in limited area mode with 6.5-km resolution and initialized with NWP analysis fields. Using P-NAER_{NSX} as the prior, we model the three-dimensional CH₄ concentration field resulting from the leaks and compare hourly outputs with observations from the ICOS and NILU sites.

Owing to meteorological uncertainty, the timing of modelled and observed plume arrival differs. To allow for this uncertainty, the modelled signals from the leaks are integrated in time for each of the 5 measurement stations (m_i , where $i = 1, \dots, 5$). The observed signals (o_i , where $i = 1, \dots, 5$) are obtained analogously after subtracting the background from each observation time series. This background and its uncertainty are estimated for each station using the average and standard deviation of the September observations before arrival of the plume. Because the concentration scales with the emissions, an emission scaling factor is calculated for each station (s_i) as:

$$s_i = \frac{o_i}{m_i} \quad (9)$$

Our posterior emissions estimate p_i is derived by:

$$p_i = s_i \times e(t) \quad (10)$$

where $e(t)$ is the time dependent P-NAER_{NSX}.

Ideally, the scaling factors for all stations would agree, but they differ, probably because of a plume location error. To capture a wide range of plausible meteorological variability, we use an ICON-ART ensemble of 40 members and an additional deterministic run. The ensemble is constructed using operational weather forecasting methods and represents 40 slightly different, equally likely, meteorological initial conditions (k). The scaling factors derived from the ensemble members vary substantially. The minimum emission scaling needed to match the observed with the modelled integrated plume signal at a station is given by $s_i = \min(s_i, k)$ (where $k = 1, \dots, 40$). This way, the dominant meteorological uncertainty is regarded by providing lower bounds for the emissions at each station. Owing to the high response of concentration distribution to the meteorological uncertainty, there are cases where

the modelled signal is close to zero owing to location error and scaling factors grow to infinity. Therefore, no upper bound can be derived.

Uncertainties aside from the meteorology are regarded as follows. For each ensemble member, the uncertainty of the prior emissions is propagated to m_i by distinguishing the contributions of emissions from 14 time intervals. The uncertainty of each contribution to m_i is bounded by the maximum relative prior uncertainty within the respective time interval. Summing these contributions yields upper bounds on the uncertainties of m_i between 1% and 10%, depending on which part of the plume is observed. Here, the P-NAER_{NSx} emission profiles representing the prior uncertainty are normalized to the total emissions because the inversion result is independent of the total prior emissions. A higher uncertainty of 6% to 34% is obtained for observations o_i due to the background subtraction.

Our emissions estimate is the highest minimum p_i derived across the measurement stations (in this case, BIR) rounded to the nearest 10 kt of CH₄. Given the time dependency of emissions $e(t)$ and allowing for meteorological transport uncertainty as used in NWP methods, this approach can only derive a lower bound of atmospheric emissions.

Inversion 4

Inversion 4 is derived from the reanalysis of a previous inversion⁸ (Supplementary Table 1), using CH₄ concentrations from four ICOS stations (BIR, NOR, HTM and UTO)^{62,63,69,72} between 26 September and 1 October 2022. We use the Stochastic Time-Inverted Lagrangian Transport model (STILT)^{73,74} to model atmospheric transport. The STILT simulation is driven by $0.25^\circ \times 0.25^\circ$ global meteorological fields from the National Centers for Environmental Prediction operational Global Forecast System⁷⁵ analysis. CH₄ concentration enhancements at the four stations are computed by subtracting the median of all September observations before 26 September from the time-series observations. The sensitivity of CH₄ enhancements at ICOS stations to CH₄ emission rates are computed with forward-mode STILT simulations by tracking the surface influence of 500 particles released from two leak points (one for the adjacent NS1A and NS1B leak sites, and one for the NS2A leak site). As for inversion 2, we solve a Bayesian inverse problem to estimate hourly CH₄ emission fluxes from the two leak points using equations (7) and (8). The Jacobian matrix H in equations (7) and (8) is the sensitivity derived from the STILT simulations.

In the previous estimate⁸, x_b were assumed to be zero because no credible prior information was available at the time of publication. Here, we use P-NAER_{NSx} for x_b . The prior error for the matrix H is considered to be the maximum uncertainty in the P-NAER_{NSx} prior for emission rates $>100 \text{ t h}^{-1}$ (about 10%), and the observation error for the matrix R is 30 ppbv. We compute the uncertainty of the posterior estimate \hat{x} by analysing the posterior error covariance matrix (\hat{S}) given by equation (11):

$$\hat{S} = (H^T \times R^{-1} \times H + B^{-1})^{-1} \quad (11)$$

Inversion 5

Inversion 5 is derived using CH₄ concentrations from three ICOS stations (BIR, NOR and HTM)^{76,77} between 26 September and 3 October 2022. We model atmospheric transport using the TNO LOTOS–EUROS chemistry transport model^{78,79} operated at $0.1^\circ \times 0.1^\circ$ resolution. Meteorological fields are derived from the short-range ECMWF forecast. The CH₄ concentration signal from non-Nord Stream sources are generated by the LOTOS–EUROS model using the CAMS-REGv5 emission inventory⁸⁰ for anthropogenic emissions and the Copernicus Atmosphere Monitoring Service global atmospheric composition forecast⁸¹ for boundary conditions. Modelled CH₄ concentrations from these sources are considered as background from which we derive CH₄ enhancements from the leaks.

We produce two LOTOS–EUROS simulations using P-NAER_{NSx} and C-NAER_{NSx}, including their uncertainty, as the prior. Each simulation

results in a total of 35 runs for each NS1 leak and 40 runs for the NS2A leak, leading to a total of 110 runs. For each simulation, a fitting routine is applied to derive an emissions estimate. The fitting is described by an $Ax = B$ system, where A is the source receptor relations, x is the hourly emission enhancement and B is the hourly measurements from the three ICOS stations. The matrix A contains the concentrations simulated in each of our runs at the location of the three ICOS towers. The $Ax = B$ system is underdetermined, and therefore a least-square fit is derived for x such that Ax is as close to B as possible. When the emission enhancements in x are multiplied with the initial emission strengths an estimate for the total emissions is obtained. The estimate uncertainty is the standard deviation across the fittings.

Inversion 6

Inversion 6 is derived from the reanalysis of previous inversions^{16,17} (Supplementary Table 1), using the temporal variation of CH₄ concentrations from two ICOS stations (BIR and NOR)^{62,63} between 26 September and 3 October 2022. We conduct atmospheric transport simulations using the CHIMERE chemistry transport model⁸², with 0.2° horizontal resolution and vertical resolution divided into 29 vertical levels from the surface up to 300 hPa. Our CHIMERE simulations are driven by the Community Inversion Framework⁸³. The meteorological fields are interpolated at the model resolution and are derived from 3-hourly operational forecasts sourced from ECMWF at a resolution of 0.15° . The CH₄ concentration signal from non-Nord Stream sources is simulated using a standard regional configuration. Anthropogenic emissions other than Nord Stream are derived from EDGARv6⁸⁴ at $0.1^\circ \times 0.1^\circ$ resolution. For natural emissions, such as natural fluxes from peatlands, inundated and mineral soils are taken from the JSBACH-HIMMELI model⁸⁵. Geological emissions are a climatology based on ref. 86 and GCP-CH₄ and scaled down to a global total of 15 Tg of CH₄ in accordance with the maximum suggested by ref. 87. Ocean CH₄ fluxes are a climatology based on ref. 88. Background concentrations at the side of the area-limited domain of CHIMERE are interpolated from the Copernicus Atmosphere Monitoring Service CH₄ reanalysis⁸⁹.

The previous estimates used a constant emission prior¹⁶, and an assumed exponential emission prior¹⁷. Our reanalysis uses C-NAER_{NSx} as the emission prior. To ensure the posterior estimates are not biased by the confidence we have with C-NAER_{NSx} values, we use C-NAER_{NSx} temporal profiles and not the value of the rate. To do so, we carry out Monte Carlo simulations by multiplying the emission rate from C-NAER_{NSx} by a random coefficient between 0 and 1.5. This allows to cover the lower and upper bounds of the C-NAER_{NSx} priors. To account for uncertainties from meteorological data, we integrate 11 meteorological datasets from the ECMWF ensemble forecast. The 11 members from the ensemble forecast represent data slightly deviated from a standard case. In addition, CATHARE modelling indicates that the gas velocity exceeds 55 m s^{-1} during the first 24 h of at all leak sites. For that same period, gas temperatures did not exceed -35°C owing to localized depressions between the pressure inside and outside the pipelines. Accordingly, we use the analytical solutions for turbulent buoyant plumes from circular sources to estimate the altitude the gas reached before dispersion.

To estimate atmospheric CH₄ emissions, we generate 10,000 distinct scenarios. Each scenario is created by picking a random meteorological dataset from the 11 members and an altitude from 10 values between 0 m and 2,000 m for each day of the leaks. Finally, for each scenario, a reduction factor randomly fixed between 0 and 1.5 is assigned. For each scenario, we compute a probability expressing how much the scenario is close to the observations. Within the Bayesian data assimilation process, we evaluate the probability of the reduction coefficient knowing the probability of the scenario. The Bayesian probability is expressed as:

$$P(x|y) \propto P(y|x) \times P(x) \times P(\text{alt}|x) \quad (12)$$

where x is the reduction coefficient, alt is the altitude reached by the gas, and y is the comparison between the simulations and the observations for the selected stations. $P(x|y)$ is assimilated to the posterior that we want to estimate, $P(x)$ is the emission prior and $P(alt|x)$ is the probability to reach an altitude knowing the rate. To evaluate equation (12), we use the analytical solutions for turbulent buoyant plumes from circular sources. The Bayesian data assimilation allows us to estimate the range and maximum probability of our posterior estimate.

Data availability

The input data decks for the CATHARE code, output data obtained from both PBREAK and CATHARE modelling, and the chemical composition of the natural gas used in our modelling³⁴ can be downloaded at <https://gitfront.io/r/StephenHarrisUNEPIMEO/Emq51iMoNq3M/Available-Data-for-Harris-et-al-Methane-emissions-from-the-Nord-Stream-subsea-pipeline-leaks/>. Ocean glider dissolved methane observations are freely accessible at observations.voiceoftheocean.org; the relevant datasets can be found by the IDs SEA070 M13, SEA070 M14, SEA070 M15, SEA056 M54, SEA056 M55, SEA056 M56 and SEA056 M57. The SOOP data are freely available via the ICOS Carbon Portal at <https://doi.org/10.18160/K3BM-8YNG>. Airborne observations obtained with the HELiPOD platform on 5 October 2022 are available under a CCBY4 license at <https://doi.org/10.18160/D0DQ-F7GE>. The data presented in this study use the EU Copernicus Marine Service Information (<https://doi.org/10.48670/moi-00010>).

Code availability

The PBREAK model, embedded within the PIPESAFE Quantitative Risk Assessment software, can be accessed via the software developer DNV at <https://www.dnv.com/>. CATHARE code licencing can be obtained at https://cathare.cea.fr/Pages/Contact/Contact_Us.aspx. The CATHARE licence is free for non-commercial use.

47. Acton, M., Baldwin, T. & Jager, E. Recent developments in the design and application of the PIPESAFE risk assessment package for gas transmission pipelines. In *Proc. 2002 4th International Pipeline Conference* 831–839 (ASME, 2002).
48. Acton, M. R., Hankinson, G., Ashworth, B. P., Sanai, M. & Colton, J. D. A full-scale experimental study of fires following the rupture of natural gas transmission pipelines. In *Proc. 2000 3rd International Pipeline Conference* V001T01A008 (ASME, 2000).
49. Acton, M., Dimitriadis, K., Potts, S. & Warhurst, K. Risk assessment of natural gas transmission pipelines at major river crossings. *Hazards* **27**, 1–12 (2017).
50. Mauger, G., Tauveron, N., Bentivoglio, F. & Ruby, A. On the dynamic modeling of Brayton cycle power conversion systems with the CATHARE-3 code. *Energy* **168**, 1002–1016 (2019).
51. Barre, F. & Bernard, M. The CATHARE code strategy and assessment. *Nucl. Eng. Des.* **124**, 257–284 (1990).
52. Bestion, D. The physical closure laws in the CATHARE code. *Nucl. Eng. Des.* **124**, 229–245 (1990).
53. Tenchine, D. et al. Status of CATHARE code for sodium cooled fast reactors. *Nucl. Eng. Des.* **245**, 140–152 (2012).
54. Lemmon, E. W., Huber, M. L. & McLinden, M. O. *NIST Standard Reference Database 23: Reference Fluid Thermodynamic and Transport Properties-REFPROP, Version 8.0* (NIST, 2013).
55. Kunz, O. & Wagner, W. The GERG-2008 wide-range equation of state for natural gases and other mixtures: an expansion of GERG-2004. *J. Chem. Eng. Data* **57**, 3032–3091 (2012).
56. Zigrang, D. J. & Sylvester, N. D. Explicit approximations to the solution of Colebrook's friction factor equation. *AIChE J.* **28**, 514–515 (1982).
57. Colburn, A. P. A method of correlating forced convection heat-transfer data and a comparison with fluid friction. *Int. J. Heat Mass Transf.* **7**, 1359–1384 (1964).
58. Siddans, R. et al. Global height-resolved methane retrievals from the Infrared Atmospheric Sounding Interferometer (IASI) on MetOp. *Atmos. Meas. Tech.* **10**, 4135–4164 (2017).
59. Knappett, D., Siddans, R., Ventress, L., Kerridge, B. & Latter, B. STFC RAL methane retrievals from IASI on board MetOp-B, version 2.0. NERC EDS Centre for Environmental Data Analysis <https://dx.doi.org/10.5285/4bbcb1722f2842c1b0a5ebc19160a863> (2022).
60. Wilson, C. et al. Contribution of regional sources to atmospheric methane over the Amazon Basin in 2010 and 2011. *Glob. Biogeochem. Cycles* **30**, 400–420 (2016).
61. Wilson, C. et al. Large and increasing methane emissions from eastern Amazonia derived from satellite data, 2010–2018. *Atmos. Chem. Phys.* **21**, 10643–10669 (2021).
62. Lund Myhre, C., Platt, S., Lunder, C. & Hermansen, O. ICOS ATC CH₄ release, Birkenes (75.0 m), 2020-09-14–2023-03-31, ICOS RI. ICOS <https://hdl.handle.net/11676/OvifL2UB53ib1KiFvWd63NS> (2023).
63. Lehner, I. & Mölder, M. ICOS ATC CH₄ release, Norunda (58.0 m), 2017-04-01–2023-03-31, ICOS RI. ICOS <https://hdl.handle.net/11676/mcZCu-5WouAxMyUJ8RJ9y5j> (2023).
64. Lund Myhre, C., Platt, S., Hermansen, O. & Lunder, C. ICOS ATC CH₄ release, Zeppelin (15.0 m), 2017-07-27–2023-03-31, ICOS RI. ICOS https://hdl.handle.net/11676/_SsoN8BWsu3N8-gSfqIMfq9e (2023).
65. Pisso, I. et al. The Lagrangian particle dispersion model FLEXPART version 10.4. *Geosci. Model Dev.* **12**, 4955–4997 (2019).
66. Tarantola, A. *Inverse Problem Theory and Methods for Model Parameter Estimation* (Society for Industrial and Applied Mathematics, 2005).
67. Lehner, I. & Mölder, M. ICOS ATC CH₄ release, Norunda (100.0 m), 2017-04-01–2023-03-31, ICOS RI. ICOS <https://hdl.handle.net/11676/QIUve7wmfKcrMMO1yuXpae4c> (2023).
68. Heliasz, M. & Biermann, T. ICOS ATC CH₄ release, Hyltemossa (150.0 m), 2017-04-17–2023-03-31, ICOS RI. ICOS https://hdl.handle.net/11676/FNZRScPT_pVnFaZirluEpFl (2023).
69. Hatakka, J. & Laurila, T. ICOS ATC CH₄ release, Utö - Baltic Sea (57.0 m), 2018-03-09–2023-03-31, ICOS RI. ICOS https://hdl.handle.net/11676/fumW3pRc4v-JBVgu_ut72193 (2023).
70. Zängl, G., Reinert, D., Rípodas, P. & Baldauf, M. The ICON (icosahedral non-hydrostatic) modelling framework of DWD and MPI-M: description of the non-hydrostatic dynamical core. *Q. J. R. Meteorol. Soc.* **141**, 563–579 (2015).
71. Schröter, J. et al. ICON-ART 2.1: a flexible tracer framework and its application for composition studies in numerical weather forecasting and climate simulations. *Geosci. Model Dev.* **11**, 4043–4068 (2018).
72. Heliasz, M. & Biermann, T. ICOS ATC CH₄ release, Hyltemossa (70.0 m), 2017-04-17–2023-03-31, ICOS RI. ICOS <https://hdl.handle.net/11676/FdkjV8DuFgh6jxrd7TSqqD2f> (2023).
73. Lin, J. et al. A near-field tool for simulating the upstream influence of atmospheric observations: the Stochastic Time-Inverted Lagrangian Transport (STILT) model. *J. Geophys. Res. Atmos.* **108**, 4493 (2013).
74. Gerbig, C. et al. Toward constraining regional-scale fluxes of CO₂ with atmospheric observations over a continent: 2. Analysis of COBRA data using a receptor-oriented framework. *J. Geophys. Res. Atmos.* **108**, 4757 (2003).
75. National Centers for Environmental Prediction/National Weather Service/NOAA/US Department of Commerce. NCEP GFS 0.25 degree global forecast grids historical archive. *Research Data Archive at the National Center for Atmospheric Research, Computational and Information Systems Laboratory* <https://doi.org/10.5065/D65D8PWK> (2015).
76. Lund Myhre, C., Platt, S., Lunder, C. & Hermansen, O. ICOS ATC CH₄ release, Birkenes (10.0 m), 2020-09-14–2023-03-31, ICOS RI. ICOS <https://hdl.handle.net/11676/75hLzzO1hVvMUgJNb4z-OnXM> (2023).
77. Lehner, I. & Mölder, M. ICOS ATC CH₄ release, Norunda (32.0 m), 2017-04-01–2023-03-31, ICOS RI. ICOS <https://hdl.handle.net/11676/KMfBLfiQaLQRO9EmAhJR960> (2023).
78. Manders, et al. Curriculum vitae of the LOTOS-EUROS (v2.0) chemistry transport model. *Geosci. Model Dev.* **10**, 4145–4173 (2017).
79. Timmermans, R. D. Evaluation of modelled LOTOS-EUROS with observational based PM10 source attribution. *Atmos. Environ. X* **14**, 100173 (2022).
80. Kuenen, J. et al. CAMS-REG-v4: a state-of-the-art high-resolution European emission inventory for air quality modelling. *Earth Syst. Sci. Data* **14**, 491–515 (2022).
81. Agustí-Panareda, A., Diamantakis, M., Bayona, V., Klappenbach, F. & Butz, A. Improving the inter-hemispheric gradient of total column atmospheric CO₂ and CH₄ in simulations with the ECMWF semi-Lagrangian atmospheric global model. *Geosci. Model Dev.* **10**, 1–18 (2017).
82. Fortems-Cheiney, A. et al. Variational regional inverse modeling of reactive species emissions with PYVAR-CHIMERE-v2019. *Geosci. Model Dev.* **14**, 2939–2957 (2021).
83. Berchet, A. et al. The Community Inversion Framework v1.0: a unified system for atmospheric inversion studies. *Geosci. Model Dev.* **14**, 5331–5354 (2021).
84. Monforti Ferrario, F. et al. EDGAR v6.0 greenhouse gas emissions. European Commission, Joint Research Centre (JRC), dataset. *European Commission* <http://data.europa.eu/89h/97a67d67-c62e-4826-b873-9d972c4f670b> (2021).
85. Raivonen, M. et al. HIMMEL v1.0: Helsinki model of methane build-up and emission for peatlands. *Geosci. Model Dev.* **10**, 4665–4691 (2017).
86. Etiope, G., Ciotoli, G., Schwietzke, S. & Schoell, M. Gridded maps of geological methane emissions and their isotopic signature. *Earth Syst. Sci. Data* **11**, 1–22 (2019).
87. Petrenko, V. V. et al. Minimal geological methane emissions during the Younger Dryas-Preboreal abrupt warming event. *Nature* **548**, 443–446 (2017).
88. Weber, T., Wiseman, N. A. & Kock, A. Global ocean methane emissions dominated by shallow coastal waters. *Nat. Commun.* **10**, 4584 (2019).
89. *Contribution to Documentation of Products and Services as Provided Within the Scope of this Contract – 2023 – Part CH₄* (Copernicus Atmosphere Monitoring Service, 2023).
90. Lawson, A. Nord Stream 2 pipeline pressure collapses mysteriously overnight. *The Guardian* <https://www.theguardian.com/business/2022/sep/26/nord-stream-2-pipeline-pressure-collapses-mysteriously-overnight/> (2022).
91. Harby, K., Chiva, S. & Muñoz-Cobo, J. L. Modelling and experimental investigation of horizontal buoyant gas jets injected into stagnant uniform ambient liquid. *Int. J. Multiph. Flow* **93**, 33–47 (2017).
92. Lund Myhre, C., Platt, S. M., Lunder, C. & Hermansen, O. ICOS ATC NRT CH₄ growing time series, Birkenes (10.0 m), 2022-03-01–2022-10-16, ICOS RI. ICOS <https://hdl.handle.net/11676/a-QqGFe7Aga6-k7Chen39EyQ> (2022).
93. Lund Myhre, C., Platt, S., Lunder, C. & Hermansen, O. ICOS ATC CH₄ release, Birkenes (50.0 m), 2020-09-14–2023-03-31, ICOS RI. ICOS https://hdl.handle.net/11676/lMSx28tDaMg1owQ5DHJOU__ (2023).
94. Lund Myhre, C., Platt, S. M., Lunder, C. & Hermansen, O. ICOS ATC NRT CH₄ growing time series, Birkenes (50.0 m), 2022-03-01–2022-10-16, ICOS RI. ICOS https://hdl.handle.net/11676/QhtU7Bpi3hW63r_P_YRETTsU (2022).
95. Lund Myhre, C., Platt, S. M., Lunder, C. & Hermansen, O. ICOS ATC NRT CH₄ growing time series, Birkenes (75.0 m), 2022-03-01–2022-10-16, ICOS RI. ICOS https://hdl.handle.net/11676/M1WVvYdMy6UtPnSvF6KKmq_L (2022).
96. Hatakka, J. & Laurila, T. ICOS ATC NRT CH₄ growing time series, Utö - Baltic Sea (57.0 m), 2022-03-01–2022-10-16, ICOS RI. ICOS https://hdl.handle.net/11676/yFO_L2onDwckHg_2194ej4Mx (2022).
97. Heliasz, M. & Biermann, T. ICOS ATC CH₄ release, Hyltemossa (30.0 m), 2017-04-17–2023-03-31, ICOS RI. ICOS <https://hdl.handle.net/11676/Le3qzCL2U56Ya2gvlZHYISR> (2023).

98. Heliasz, M. & Biermann, T. ICOS ATC NRT CH₄ growing time series, Hyltemossa (30.0 m), 2022-03-01–2022-10-16, ICOS RI. ICOS <https://hdl.handle.net/11676/19QSN5WCe3fqCzL0iTwLU8la> (2022).
99. Heliasz, M. & Biermann, T. ICOS ATC NRT CH₄ growing time series, Hyltemossa (70.0 m), 2022-03-01–2022-10-16, ICOS RI. ICOS <https://hdl.handle.net/11676/lv2Wf-vf84LsT73z6kWFJgV4> (2022).
100. Heliasz, M. & Biermann, T. ICOS ATC NRT CH₄ growing time series, Hyltemossa (150.0 m), 2022-03-01–2022-10-16, ICOS RI. ICOS <https://hdl.handle.net/11676/-uYDRenkP8mfYPJLhEkmx9Ko> (2022).
101. Lehner, I. & Mölder, M. ICOS ATC NRT CH₄ growing time series, Norunda (32.0 m), 2022-03-01–2022-10-16, ICOS RI. ICOS https://hdl.handle.net/11676/1hIMJfGI_pDmu8CLT2DNB4R (2022).
102. Lehner, I. & Mölder, M. ICOS ATC NRT CH₄ growing time series, Norunda (58.0 m), 2022-03-01–2022-10-16, ICOS RI. ICOS <https://hdl.handle.net/11676/vZQwyfmyDblCceVXxEefe7h> (2022).
103. Lehner, I. & Mölder, M. ICOS ATC NRT CH₄ growing time series, Norunda (100.0 m), 2022-03-01–2022-10-16, ICOS RI. ICOS <https://hdl.handle.net/11676/DHD1wLPlqB2Fo-NlWVBHed5> (2022).
104. *Espoo Report: Nord Stream 2* W-PE-EIA-POF-REP-805-040100EN (Rambøll A/S, 2017).
105. The first Nord Stream 2 string filled with technical gas. *Nord Stream 2* <https://web.archive.org/web/20220120045759/https://www.nord-stream2.com/media-info/news-events/the-first-nord-stream-2-string-filled-with-technical-gas-154/> (2021).
106. Second Nord Stream 2 string filled with technical gas. *Nord Stream 2* <https://web.archive.org/web/20220119203619/https://www.nord-stream2.com/media-info/news-events/second-nord-stream-2-string-filled-with-technical-gas-156/> (2021).
107. *Espoo Atlas: Nord Stream 2* W-PE-EIA-POF-DWG-805-040100EN (Rambøll A/S, 2017).
108. *Erdgas-Orientierungswerte 2022* (Open Gas Europe, 2023); https://oge.net/_Resources/Persistent/b/b/3/e/bb3e99d510987606aafbf73c09ea23f60c03248f/OGE%20Erdgas-Orientierungswerte%202022%20Stand%2021_03_2023.pdf.

Acknowledgements This research was funded in the framework of UNEP's International Methane Emissions Observatory (IMEO). We thank E. Nisbet and D. Zavala-Araiza for comments on the paper; and A. Sundberg from the Swedish Coast Guard (Kustbevakningen) for providing us with sea foam patch diameter measurements for the NS1A and northern NS2A leak sites. We thank the Danish Energy Agency (Energistyrelsen) for supplying information on pipeline pressures. The CATHARE code (<https://cathare.cea.fr>) is developed by the CEA in the framework of the NEPTUNE project, supported by the CEA, EDF (Electricity of France), FRAMATOME and IRSN (French Radioprotection and Nuclear Safety Institute). B.Y.Q., L.C.B. and M.M. thank Alseamar for loan of the Franatech METS sensor and J. Gronemann at Franatech for support in processing the methane data. B.Y.Q.'s time was funded by the Voice of the Ocean Foundation, EU GROOM II grant (ID 951842), and Swedish Formas grant 2022-01536. Operation of DE-SOOP-Finnmaid was supported through ICOS by the German Federal Ministries for Education and Research (BMBF) and Digital and Transport (BMDV). The University of Gothenburg provided funding for ship time aboard the RV *Skagerak*. IASI retrievals used in inversion 1 were produced using JASMIN, the UK collaborative data analysis facility. Development of the version of RAL's IASI retrieval scheme from which Nord Stream methane data were produced was funded through UK NCEO and ESA's Methane+ project (ESA contract number 4000129987/20/I-DT). M.D. was in part funded through the ESA MethaneCAMP project. Inversion 1 model simulations

were carried out using ARC4, part of the High-Performance Computing facilities at the University of Leeds, UK. EUMETSAT provided data for MetOp-B IASI, MHS and AMSU-A data, and ECMWF provided meteorological data used in inversion 1. Inversion 1 work was funded by the Natural Environment Research Council through its grants to the UK National Centre for Earth Observation (NCEO; NERC grant numbers NE/R016518/1 and NE/N018079/1). HELIPOD measurements in October 2022 were partly funded by UNEP's IMEO, partly by DLR, and the measurements in November 2022 were funded by the German Research Foundation under grant LA 2907/19-1. Work conducted as part of the inversion 2 analysis was funded by ReGAME (NFR 325610), ICOS (NFR 296012) and EYE-clima (Horizon Europe 101081395). I. Pisso and S.E. acknowledge funding from Reduch4e (NKL-2304). Inversion 3 analysis was supported by BMDV with HoTC (grant 50EW2013A) and by BMBF with ITMS (grant 01LK2102B). Y.Z. acknowledges funding by the National Key Research and Development Program of China (2022YFE0209100) and the National Natural Science Foundation of China (42275112).

Author contributions S.J.H., S.S., J.L.F. and A.C. conceptualized the study. S.J.H. wrote the paper, coordinated input from all authors and oversaw data sharing between co-authors. All authors reviewed the paper and assisted in shaping the analyses. N.V.S., T.M.F., P.B., C.B. and C.M. assisted in the compilation of bottom-up estimates and pipeline physical parameters. J.L. performed the PBREAK simulations, assisted in the compilation of pipeline physical parameters and wrote the accompanying Methods. R.P., T.B., F.D., G.M. and A.M. performed the CATHARE code simulations, assisted in the compilation of pipeline physical parameters and wrote the accompanying Methods. K.A., E. Damm, G.B., M.M., L.C.B., B.Y.Q., G.R. and H.C.B. provided data from marine estimates, shaped interpretations of the fate of methane in the water column and wrote parts of the 'Marine and ship-based estimates' section. F.R., A.L., J.M., F.P. and A.R. provided data from airborne estimates, shaped interpretations of the fate of methane in the water column and atmosphere and wrote the 'Airborne estimate' section. J.-P.W.M. provided insights into GHGSat observations and wrote parts of the 'Satellite point-source estimates' section. M.D., J.D.M., I.A. and D.J.V. provided insights into L8 and S-2B observations and wrote parts of the 'Satellite point-source estimates' section. M.J., F.J., F.L. and Y.Z. provided insights into S-2B observations, wrote parts of the 'Satellite point-source estimates' section, and performed and wrote the Methods for inversion 4. C.W., M.P.C., E. Dowd, W.F., B.J.K., D.P.M., J.J.R., R.S. and L.J.V. provided insights into the IASI observations and wrote parts of the 'Satellite estimates using IASI' section. I.I.-L., L.G. and C.R. assisted in the interpretation of all satellite estimates. I. Pisso, S.E., S.M.P., N.S., R.L.T., M.C. and N.E. performed and wrote the Methods for inversion 2. A.K.K.-W., V.B., A.S. and B.M. performed and wrote the Methods for inversion 3. H.D.v.d.G., E. Dammers and R.N. performed and wrote the Methods for inversion 5. A.B., I.K., I. Pison, M.R. and P.C. performed and wrote the Methods for inversion 6.

Competing interests The authors declare no competing interests.

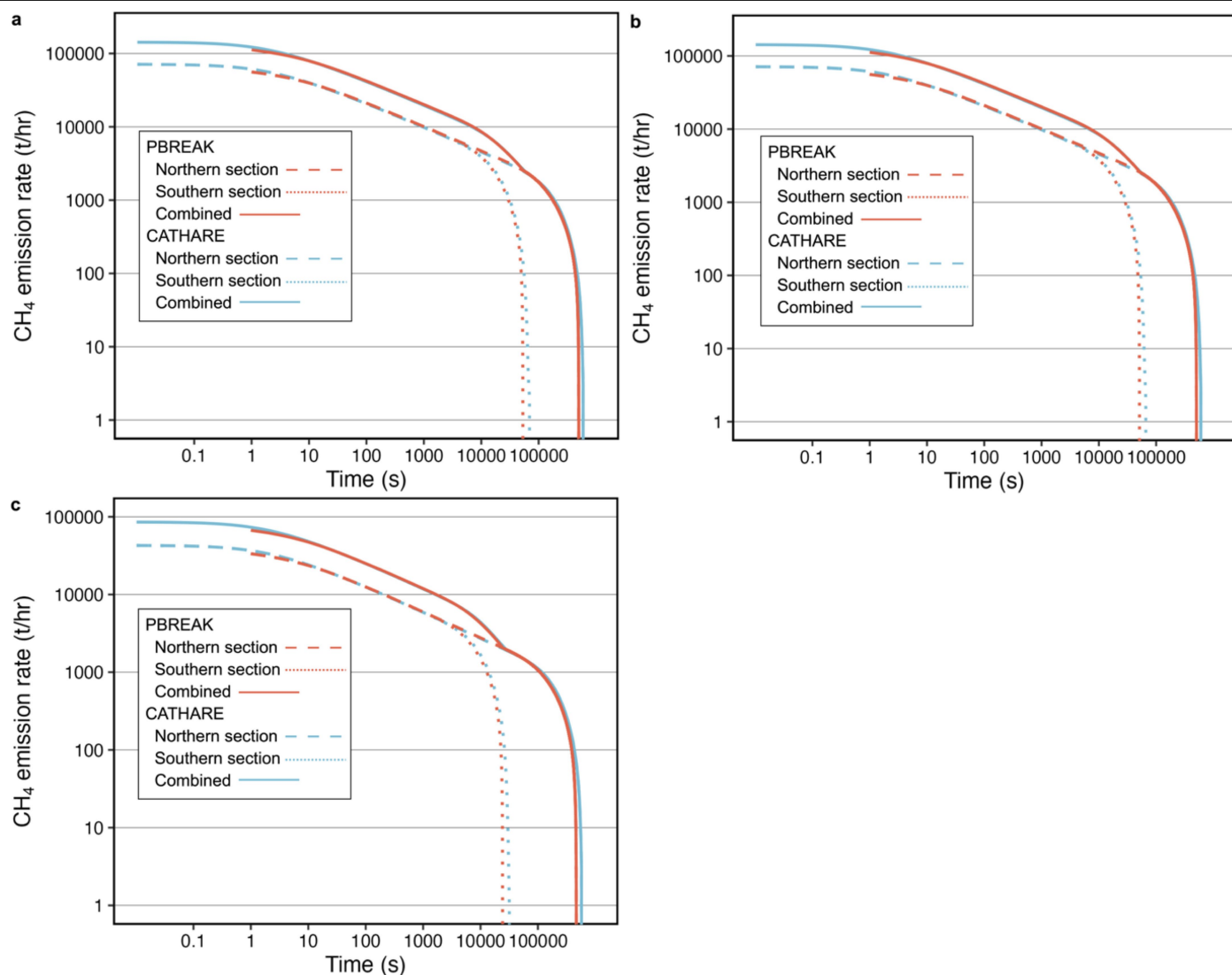
Additional information

Supplementary information The online version contains supplementary material available at <https://doi.org/10.1038/s41586-024-08396-8>.

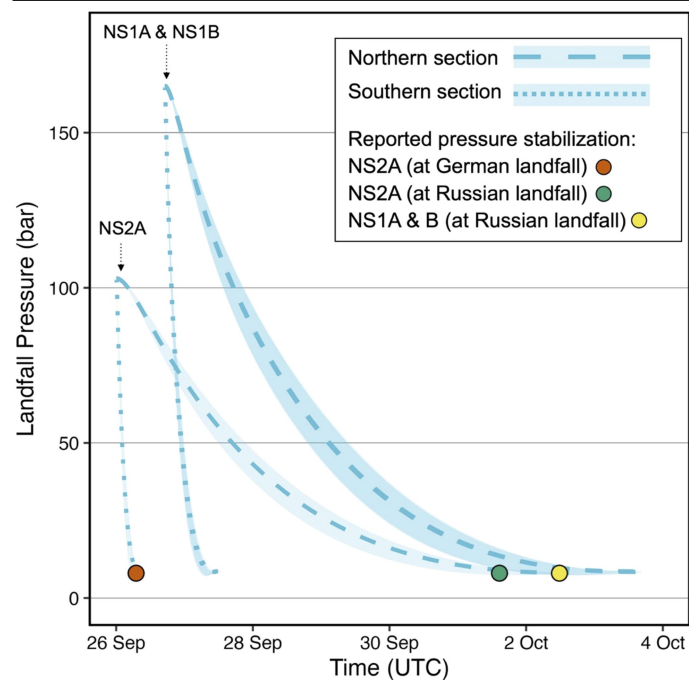
Correspondence and requests for materials should be addressed to Stephen J. Harris or Andreea Calcan.

Peer review information *Nature* thanks John Kessler and the other, anonymous, reviewer(s) for their contribution to the peer review of this work. Peer reviewer reports are available.

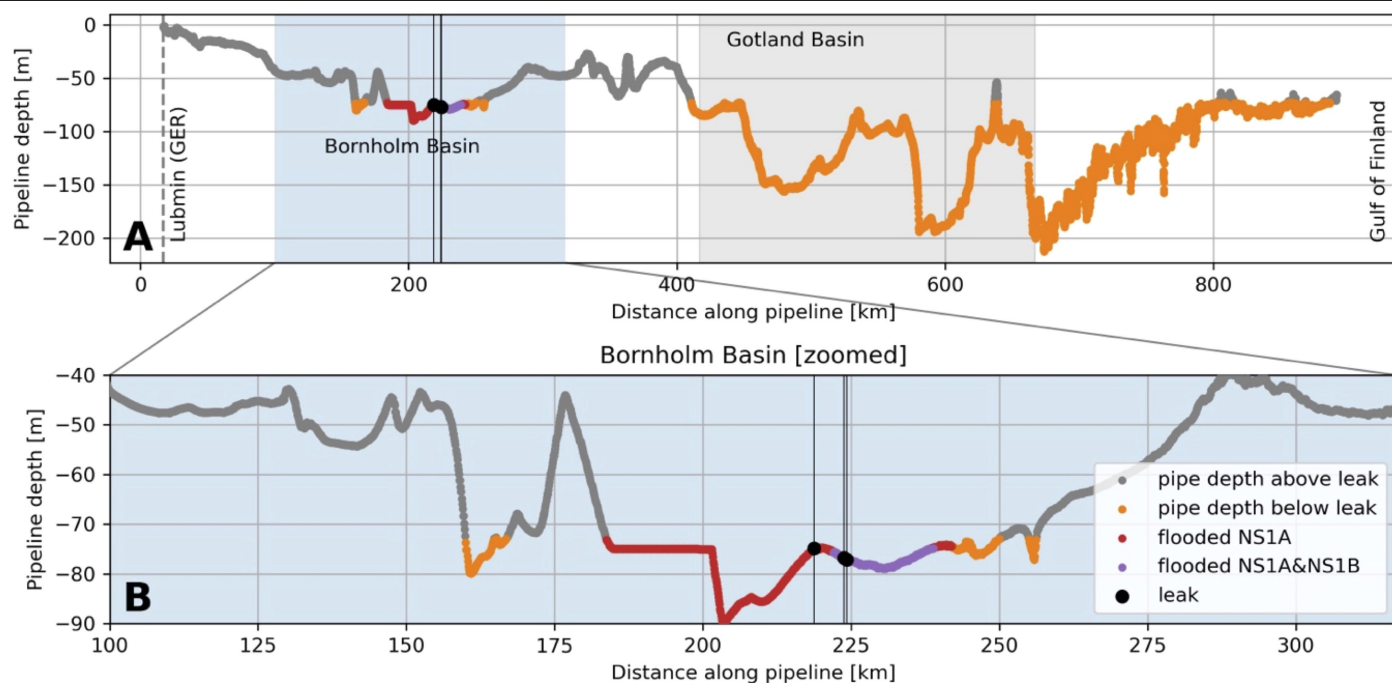
Reprints and permissions information is available at <http://www.nature.com/reprints>.



Extended Data Fig.1 | CH₄ emission rates for the (A) NS1A pipeline, (B) NS1B pipeline and (C) NS2A pipeline sections modelled using PBREAK (orange) and CATHARE (blue). Note we do not show shaded uncertainty bounds (as in Figs. 3 and 4) to maintain figure clarity.

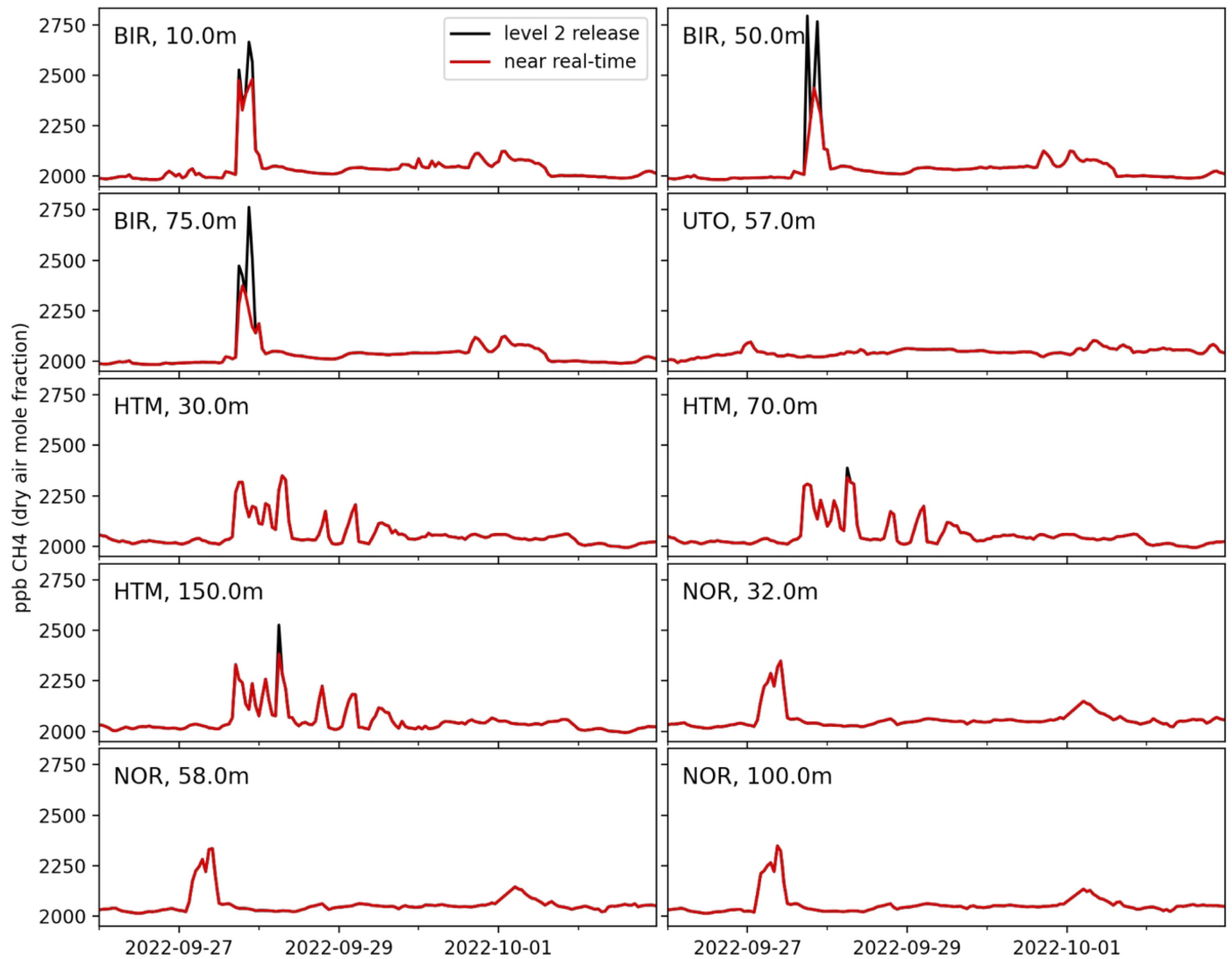


Extended Data Fig. 2 | Comparison of simulated landfall pipeline pressures for NS1A, NS1B and NS2A obtained using CATHARE with reported pressure data. Shaded regions represent the upper and lower uncertainty bounds for landfall pressure. On 26 September 2022, ref. 90 reported a pressure drop in the NS2A pipeline overnight with pressure falling to 7 bar at landfall in Lubmin, Germany. Thus, a stabilized pressure was likely obtained before daybreak around 07:00 UTC (brown circle). On 01 October 2022 at 13:38 UTC, the DEA were informed by pipeline operators that pressure stabilization in the NS2A pipeline had occurred at Russian landfall (green circle) (Danish Energy Agency, personal communication). On 02 October 2022 at 10:42 UTC, the DEA were informed by pipeline operators that pressure stabilization in the NS1 pipelines had occurred at Russian landfall (yellow circle) (Danish Energy Agency, personal communication). These reported timelines are broadly consistent with our landfall pressure time series computed using CATHARE.



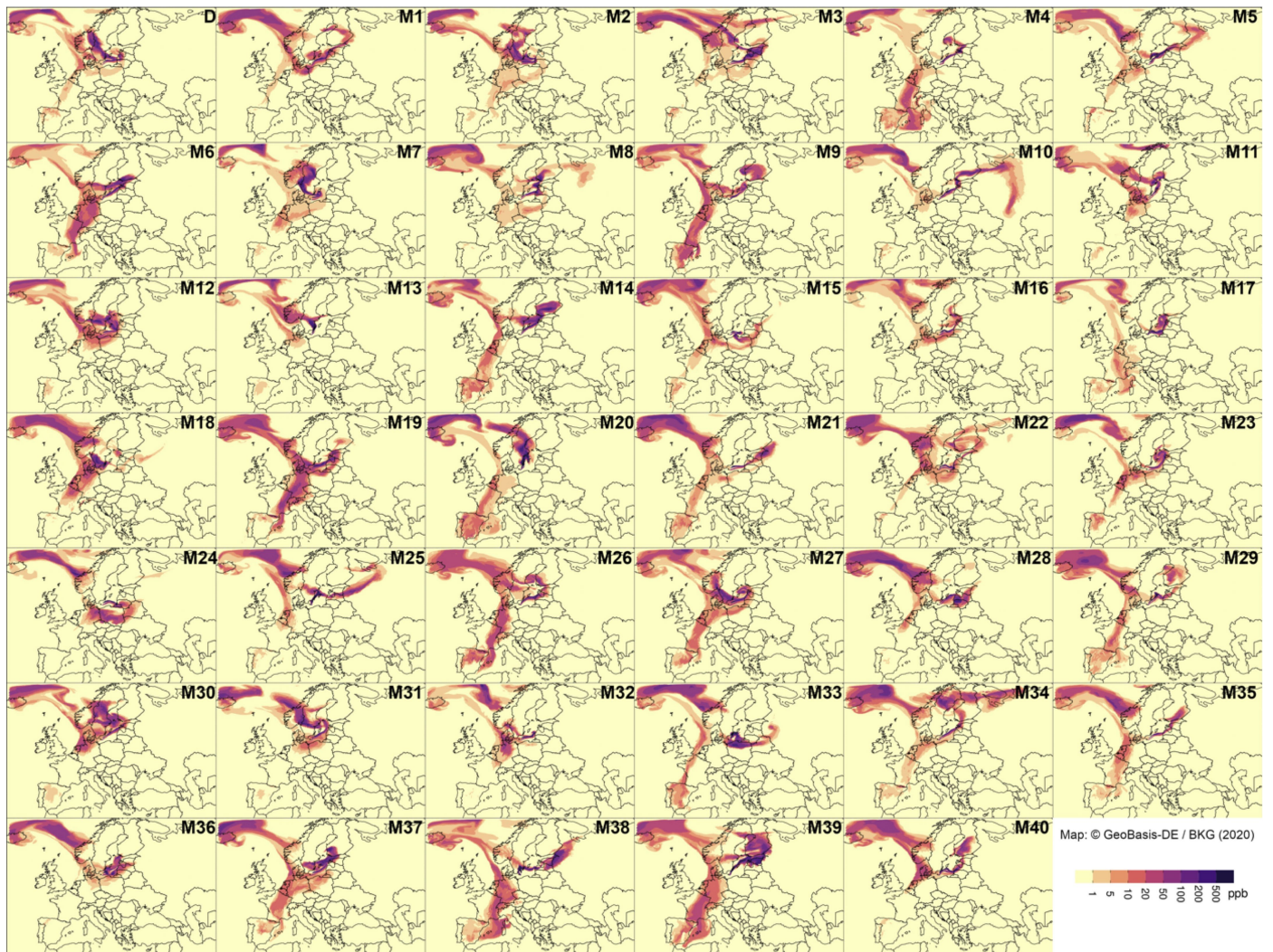
Extended Data Fig. 3 | Seawater displacement of pipeline gas using Nord Stream 1 bathymetric depth profiles (A) between Lubmin (Germany) and the Gulf of Finland, and (B) within the Bornholm Basin. During the gas leaks, some sections of the pipelines were most likely flooded. We computed the Froude number⁹¹ at the break sites from CATHARE results (Supplementary Method 1). The Froude number remains greater than 1 during the majority of the CATHARE simulation and falls below 1 only at low break velocity and flowrate (less than 100 t/hr). This indicates that the break flow inertia was enough to prevent seawater entering in the pipeline for the vast majority of the pipeline natural gas release. Therefore, we assume that the flooding occurred only in the parts of the pipeline that are located deeper than the leaks. The pipeline sections higher than the leaks, or that are deeper than the leaks but located behind a higher located sill, were not flooded because the remaining natural gas pressure would have kept additional seawater from entering. Using

the pipelines' coordinates³⁰, we compute the length of the pipeline that is located deeper than the individual leaks and is not disconnected by higher sections. Note that only detailed coordinates for the NS1 pipeline were available, so the estimations are limited to NS1A and NS1B. Using the pipeline diameter (1153 mm) and the derived flooded lengths (51 km and 11 km), the flooded volume is 53,549 m³ and 11,605 m³ for NS1A and NS1B, respectively. We correspondingly estimate that 373 t natural gas (347 t CH₄) is displaced. This result is sensitive for changes of the leak depth. Here we derived the leak depth and pipeline depths only by co-location with the bathymetry. However, the pipeline could be trenced into the seafloor or run slightly elevated. To account for this uncertainty, we varied the leak depth by ± 2 m, which changes the displaced CH₄ between 137 t to 459 t. Considering the leaks in NS2A also occurred in the Bornholm Basin at a depth >70 m, it is reasonable to expect that the total displaced CH₄ was less than 1 kt across the three pipelines.



Extended Data Fig. 4 | Time series of CH_4 mixing ratios. Near Real-Time (NRT; red) and Level 2 release (black) time series of CH_4 mixing ratios at different sampling heights from selected ICOS stations between 26 September and 3 October 2022 (BIR 10 m^{76,92}, 50 m^{93,94}, 75 m^{62,95}; UTO 57 m^{69,96}; HTM 30 m^{97,98}, 70 m^{72,99}, 150 m^{58,100}; and NOR 32 m^{77,101}, 58 m^{63,102}, 100 m^{67,103}). The ICOS time series data demonstrate that CH_4 enhancements from the Nord Stream plumes

were detected only briefly between 26 September and 3 October at several stations. Discrepancies between NRT and Level 2 release CH_4 mixing ratios are evident at the BIR, UTO and HTM stations. Initial tall tower estimates^{8,15–18} were based on NRT datasets, while the tall tower estimates presented in this study are derived from the Level 2 release data.



Extended Data Fig. 5 | Near ground (~20–60 m height) CH₄ plumes from the Nord Stream pipeline leaks modelled for 1 Oct 2022 at 00:00 UTC with ICON-ART^{70,71} deterministic (D) and ensemble (M1–M40) runs in Inversion 3 using the operational ICON deterministic and ensemble meteorological fields from the operational NWP (Deutscher Wetterdienst). Whirlpool-like meteorological conditions across the Baltic region during the emission event made meteorological forecasting challenging. In Inversions 3 and 6, we use meteorological ensembles of 40 and 11 members, respectively, to account for

meteorological uncertainties (Methods). The scaling factors derived from the ensemble members vary substantially in both inversions, likely because of uncertainty in the plume location. The 40 different meteorological ensembles used in Inversion 3 illustrated here are all equally likely, demonstrating the uncertainty associated with comparing simulated plumes to ICOS station time series data throughout the event. The background map is plotted using the country shape data from the German Federal Agency for Cartography and Geodesy (BKG).

Article

Extended Data Table 1 | Input variables used in the PBREAK and CATHARE simulations

Input variables*	Pipeline(s)	Value (unit)	Reference(s)
Initial pressure†	NS1A, NS1B	165 barA	5, 26, 104 & Danish Energy Agency, personal communication
	NS2A	103 barA	5, 105, 106 & Danish Energy Agency, personal communication
Initial gas temperature‡	NS1A, NS1B, NS2A	5 ± 2.5 °C	107
Inner Diameter§	NS1A, NS1B, NS2A	1153 mm	26
Rupture Depth	NS1A	77 ± 2 m	30
	NS1B	75 ± 2 m	30
	NS2A	72 ± 2 m	30
Distance from rupture to Russian landfall¶	NS1A#	1000 ± 5 km	26 & 27
	NS1B*	1006 ± 5 km	26 & 27
	NS2A**,††	1080 ± 20 km	26
Distance from rupture to German landfall¶	NS1A#	224 ± 5 km	26 & 27
	NS1B*	218 ± 5 km	26 & 30
	NS2A**,††	150 ± 20 km	26
Pipe roughness	NS1A, NS1B, NS2A	15 µm	26 & 27
Percentage mass of CH ₄ in the gas mixture‡‡	NS1A, NS1B, NS2A	93 ± 2 %	34 & 108

*Uncertainty bounds are only provided for variables that have not been explicitly reported in the literature which required us to estimate their values independently. †Initial pressures in the pipelines are taken directly from values reported by pipeline operators to the Danish Energy Agency (DEA) (Danish Energy Agency, personal communication). Pressure values for NS1 pipelines are corroborated by the steady state shut-in settle-out pressure reported in refs. 26,104. This pressure occurs when the pipelines are fully pressurized with gas but remain inactive, with no flow. The pressures used in our modelling of NS1A, NS1B and NS2A pipelines are consistent with natural gas volumes reported by pipeline operators to the DEA^{5,105,106} (see Supplementary Table 1). All pressures are reported in Absolute bar (barA). ‡Estimated using average seawater temperatures measured over 15 years in the Baltic Sea¹⁰⁷. We used multi-year average temperatures over the entire Baltic Sea given the pipelines run over multiple oceanographic Basins. We have assigned an uncertainty of ±2.5 °C to this value to reflect the typical range experienced at the associated depths in the Baltic Sea. §Taken directly from measurements reported in ref. 26. Our simulations assume the orifice size at the rupture sites were equal to the reported inner diameter of the pipelines given the pipelines were reported to have completely ruptured²¹. ||Estimated by geospatially locating the coordinates of the leak sites to the nearest subsea terrain depths provided in the European Marine Observation and Data Network (EMODnet) Digital Terrain Model (DTM) database³⁰. Reported depth errors in the EMODNet DTM used for the geolocated locations are below ±1m. We conservatively assign ±2m uncertainty to our depth estimates to exceed these values by a factor of two. ¶Note we do not vary the total pipeline length in our sensitivity analyses (see Methods), just the distances either side of the rupture points. #Given the rupture for NS1A occurred in the Swedish Economic Exclusion Zone (EEZ), pipeline lengths reported in ref. 26 indicate the rupture likely occurred <1004.9km from Russian landfall. Based on the coordinates of the leaks, we estimate there was approximately 5km distance (by surface) between the leak and the Swedish EEZ boundary. We therefore estimate the rupture occurred around 1000km from Russian landfall. We assign an uncertainty of ±5km to conservatively account for the fact the distances reported in ref. 26 may have changed due to final optimisation of the pipeline route. *Given the rupture for NS1B occurred in the Danish EEZ, pipeline lengths reported in ref. 26 indicate the rupture likely occurred >1004.9km from Russian landfall. The coordinates provided in ref. 26 indicate there was approximately 6km distance between the NS1A and NS1B leak sites. We therefore estimate the rupture occurred around 1006km from Russian landfall. Like NS1A, we assign an uncertainty of ±5 km. **The exact route of the NS2A pipeline is not known. Previous attempts by ref. 3 to cross-verify surface-level distances between the rupture points and landfall (calculated to be 1210 km) with the reported pipeline length (1230 km) were unsuccessful. Accordingly, we assigned a higher uncertainty of ±20 km to this distance. ††The distances reported refer to the southernmost NS2A leak site. ‡Note the value reported here (93% by mass) differs to that reported in Extended Data Table 2 (96% molar) due to the different reported units. The uncertainty in this value (±2% by mass) is a conservative estimate of variations in Russian Natural gas reported for 2021³⁴ and 2022¹⁰⁸, which differ by less than 1% molar.

Extended Data Table 2 | Properties of natural gas mixture used in PBREAK and CATHARE modelling

Component (unit)	Natural gas mixture used in PBREAK*	Natural gas mixture used in CATHARE†
Methane (% molar)	96.39	96.39
Nitrogen (% molar)	00.29	00.29
Carbon dioxide (% molar)	00.37	00.37
Ethane (% molar)	02.81	02.95
Propane (% molar)	00.07	00.00
I-Butane (% molar)	00.04	00.00
N-Butane (% molar)	00.01	00.00
I-Pentane (% molar)	00.01	00.00
N-Pentane (% molar)	00.00	00.00
N-Hexane (% molar)	00.01	00.00
Molar Weight (g/mol)	16.63	16.59
Density at 165 bar and 5°C (kg/m³) (Given by GERG-2008 EOS ^{§§})	160.9‡	160.4
Density at 103 bar and 5°C (kg/m³) (Given by GERG-2008 EOS ^{§§})	95.09‡	94.77

*Derived from average chemical compositions of Russian natural gas reported for 2021 in ref. 34.
†The gas mixture is simplified from ref. 34. CATHARE simulations do not consider components in the mixture that make up less than 0.1%. ‡Used in Eq. 1 (ρ_{NSM}); see Methods.

Extended Data Table 3 | Bottom-up inventory estimates derived from pipeline physical volumetric calculations and comparison with PBREAK and CATHARE model outputs

	Method	NS1A	NS1B	NS2A	Total
Initial pipeline inventories (kt CH ₄) [*]	Volumetric calculation	191 ± 5	191 ± 5	114 ± 3	496 ± 14
Simulated pipeline emissions (kt CH ₄)	PBREAK	179 ± 5	179 ± 5	99 ± 3	457 ± 14
	CATHARE	183 ± 5	183 ± 5	106 ± 3	472 ± 14
Simulated mass remaining in pipelines (kt CH ₄)	PBREAK	8 ± 0	8 ± 0	7 ± 0	23 ± 1
	CATHARE	8 ± 0	8 ± 0	7 ± 0	23 ± 1
Mass discrepancy (%) [†]	PBREAK	2 ± 0	2 ± 0	6 ± 0	3 ± 0
	CATHARE	0.3 ± 0	0.3 ± 0	0.3 ± 0	0.3 ± 0

Differences of 1kt CH₄ in the totals can occur due to rounding errors. ^{*}See Methods. Computed using parameters derived from Extended Data Tables 1 and 2. [†]Mass discrepancy = (Initial pipeline inventory – Simulated pipeline emissions – Mass remaining in pipelines) / Initial pipeline inventory. See Supplementary Discussion 3.

Extended Data Table 4 | Top-down estimates of atmospheric CH₄ emissions from the Nord Stream pipeline leaks and comparison with simulated atmospheric emissions (NAER and NAE)

Top-down method	Time measurement is valid*	Leaks	CH ₄ emissions estimate	P-NAER _{NS2A} (t/hr)	C-NAER _{NS2A} (t/hr)	P-NAE _{All} (kt)	C-NAE _{All} (kt)
Satellite							
IASI - Inversion 1	28/09/22 00:00	All	281 – 346 kt	Not applicable	Not applicable	311 – 326	301 – 336
	26/09/22 07:30	All	30 ± 1 kt [†]	Not applicable	Not applicable	32 – 35	31 – 36
IASI - IME Method ¹⁴	27/09/22 19:30	All	16 ± 1 kt [†]	Not applicable	Not applicable	293 – 308	284 – 318
	28/09/22 07:30	All	161 ± 4 kt [†]	Not applicable	Not applicable	336 – 352	325 – 360
	28/09/22 19:30	All	77 ± 2 kt [†]	Not applicable	Not applicable	366 – 384	355 – 390
GHGSat-C1 ¹³	30/09/22 10:27	NS2A (NS2A [‡])	84 ± 24 t/hr	84 – 113 (75 – 101 [‡])	117 – 195 (104 – 174 [‡])	Not applicable	Not applicable
GHGSat-C4 ¹³	30/09/22 12:54	NS2A (NS2A [‡])	24 ± 8 t/hr	72 – 101 (64 – 90 [‡])	105 – 182 (93 – 162 [‡])	Not applicable	Not applicable
S-2B ⁸	30/09/22 10:07	NS2A (NS2A [‡])	72 ± 38 t/hr	86 – 115 (77 – 102 [‡])	117 – 195 (104 – 174 [‡])	Not applicable	Not applicable
L8 and S-2B ensemble ¹²	29/09/22 09:56 (L8) and 30/09/22 10:07 (S-2B)	NS2A (NS2A [‡])	502 ± 464 t/hr	85 – 258 (76 – 230 [‡])	117 – 348 (104 – 310 [‡])	Not applicable	Not applicable
Tall tower inversions							
Inversion 2	30/09/22 22:00	All	217 – 317 kt	Not applicable	Not applicable	426 – 447	430 – 456
Inversion 3	1/10/22 00:00	All	≥ 230 kt [§]	Not applicable	Not applicable	427 – 448	432 – 457
Inversion 4	1/10/22 11:00	All	410 ± 19 kt	Not applicable	Not applicable	431 – 452	439 – 463
Inversion 5	3/10/22 00:00	All	740 ± 134 kt	Not applicable	Not applicable	434 – 456	448 – 470
Inversion 6	3/10/22 23:00	All	155 – 450 kt	Not applicable	Not applicable	434 – 456	448 – 471
Ensemble mean [¶]	30/09/22 22:00 to 3/10/22 23:00	All	430 ± 216 kt	Not applicable	Not applicable	426 – 456	430 – 471

*All dates are provided in the format dd/mm/yy hh:mm UTC. †Consist of partial plume observations due to cloud cover and/or are underestimates due to the inability for the IME method to account for IASI's vertical sensitivity, which is highest in the upper troposphere. Estimates are therefore not used to verify our simulated atmospheric emissions. ‡Adjusted emission rate assuming 89% of emissions were released at the southern NS2A leak site based on the ref. 3 analysis. The adjusted estimates are discussed further in Supplementary Discussion 1. §For the stations we obtain minimum estimates of 228 kt ± 16 kt (BIR), 96 kt ± 22 kt (NOR), 60 kt ± 13 kt (HTM), 54 kt ± 8 kt (NILU), and 72 kt ± 31 kt (UTO). Therefore, our best minimum estimate for the Nord Stream emission by 1 October 2022 is ≥230 kt CH₄ (rounded to nearest 10 kt; see Methods). ||Note that a maximum probability at 300 kt CH₄ is derived through the Bayesian data assimilation. ¶Mean does not include Inversion 3, which only provides a minimum estimate. Where ranges are provided, a central estimate is taken (e.g., Inversion 2 is treated as 267±50 kt, and Inversion 6 as 303±148).